Vibration-based Damage Detection in Laminated Composite Beams Using Spectral Finite Element Method and Genetic Algorithm

Mohammad Delpasand Moghadam

A Thesis

in the Department of

Building, Civil and Environmental Engineering

Presented in Partial Fulfillment of the Requirements

for the Degree of

Master of Applied Science (Civil Engineering)

at Concordia University

Montreal, Quebec, Canada

November, 2021

CONCORDIA UNIVERSITY

School of Graduate Studies

This is to certify that the thesis prepared

By: Mohammad Delpasand Moghadam

Entitled: Vibration-based Damage Detection in Laminated Composite Beams Using Spectral Finite Element Method and Genetic Algorithm

and submitted in partial fulfillment of the requirements for the degree of

Master of Applied Science (Civil Engineering)

complies with the regulations of the University and meets the accepted standards with respect to originality and quality.

Signed by the final examining committee:

_____Chair

Dr. Biao Li

_____Examiner

Dr. Farjad Shadmehri

_____Thesis Supervisor(s)

Dr. Emre Erkmen

_____Thesis Supervisor(s)

Dr. Rajamohan Ganesan

Approved by _____

Dr. Ashtoush Bagchi Chair of Department of Building, Civil, and Environmental Engineering

_____2022 _____

Dr. Mourad Debbabi Dean of School of Engineering

ABSTRACT

Vibration-based damage detection in laminated composite beams using Spectral Finite Element Method and Genetic Algorithm

Mohammad Delpasand Moghadam

Damage detection requires non-destructive testing of structures. Vibration-based damage detection techniques identify damage based on changes in the vibration features such as natural frequencies and mode shapes. Detecting damage requires solving an inverse problem using an analysis tool that is used as a simulator to produce possible damage cases and an optimization algorithm to find the closest model to the observed vibration features. Capturing some damage cases, such as delamination, is more difficult than others in the way that delamination is revealed in higher modes of vibration. Standard Finite Element Method requires a huge computational effort to obtain natural frequencies and mode shapes. Spectral Finite Element method that benefits from frequency-dependent shape functions, is adopted in this study as the analysis tool to model the dynamic behaviour of laminated composites. A discussion is given on the observations from the output of Spectral Finite Element method and a method is suggested to calculate the complete response of the structure based on the results of Spectral Finite Element analysis. The Wittrick-Willams procedure has been implemented to identify the natural frequencies from the frequency-dependent dynamic stiffness matrix of the system. The effect of delamination on natural frequencies of vibration of delaminated composites are studied. The Genetic Algorithm has been used to develop a damage detection tool that searches for the closest model to the observed frequencies and mode shapes.

Acknowledgments

I would like to express my gratitude to my supervisors, Dr. Emre Erkmen and Dr. Rajamohan Ganesan who assisted me patiently and kindly with their knowledge, time, support, and guidance.

I would like to thank my lovely parents and sister for their endless support during my past 17 years of continuous studying. The past two years away from you, reminded me of how much love and appreciation I hold in my heart for you. Hopefully we can reunite very soon.

Last one goes to my friends who inspired, taught and sustained me everyday. Even though we are all around the world, you will always have a special place in my heart.

Contents

List of Figures

List of Tables

Chapter 1

Introduction

1.1. Motivation

Damage detection requires non-destructive testing. Among different damage detection techniques those that identify the damage based on changes in the natural frequencies of the system are widely adopted. Detection of the damage location and its severity based on the observed frequency change, however, is an inverse problem where usually a search algorithm and a model update procedure are required to match the output of a damaged model with the observations. Capturing small damage requires analysis at higher frequencies. In special cases of damage, like delamination in laminated composite beams, high frequency analysis gains more importance. Many combinations of location and severity of damage are possible and the one with the closest dynamic properties, natural frequencies, and mode shapes, to the observed values in the dynamic test, should be chosen. The relationship between the inputs (location and severity of damage) and output (difference in dynamic properties) is a complicated function. The genetic algorithm is adopted in this study to optimize the process of searching for the closest model to the target data in such a complicated space. Wavelengths get shorter at higher frequencies, therefore, the standard finite element simulation of wave propagation, requires a high resolution of the discretization. Using standard finite element approaches, this may rapidly exceed the available computer resources, rendering the numerical simulations unfeasible. Especially since the analysis needs to be repeated many times to find the best model that fits the observed vibration features. To avoid limitations of FEM in numerical modelling, the spectral element method has been adopted by many researchers as a viable option, in which the element shape functions are built based on the frequency content considered in the analysis. The natural frequencies show up in the transient response of the structure. Solving the system of equations of the spectral analysis in the frequency domain and transforming it back to the time domain, does not affect the free vibration features like mode shapes and natural frequencies. The effect of damage on free vibration properties of structures, led to more in-depth investigation in the literature in obtaining the transient solution based on the steady-state solution. Free vibration features should be calculated separately by solving a transcendental

eigenvalue problem and then added to the final solution. The advantage of Spectral Finite Element method in fast computation of natural frequencies was motivating to build a dynamic analysis tool for delaminated composite beams.

1.2. Scope of the thesis

The scope of the analysis is kept to linear and elastic vibration of beams. Two types of spectral elements are studied. Spectral bar element that captures the axial deformation and Spectral Euler-Bernoulli beam element that captures the bending deformation. The mentioned beam and bar elements are combined to create a frame element to capture the axial, transverse and rotational displacements using one element. The axial behaviour is assumed to be uncoupled from the transverse and rotational displacements. To ensure that the uncoupled assumption is true when the frame element is used to model laminated composite beams with and without delamination, the laminated composite cases are limited to symmetric cases. For delaminated composite beams, only delaminated cases with mid-plane delamination are considered under the condition that the layers on the top and bottom of the delamination are also symmetric. This assumption is shown in Figure 1.1.

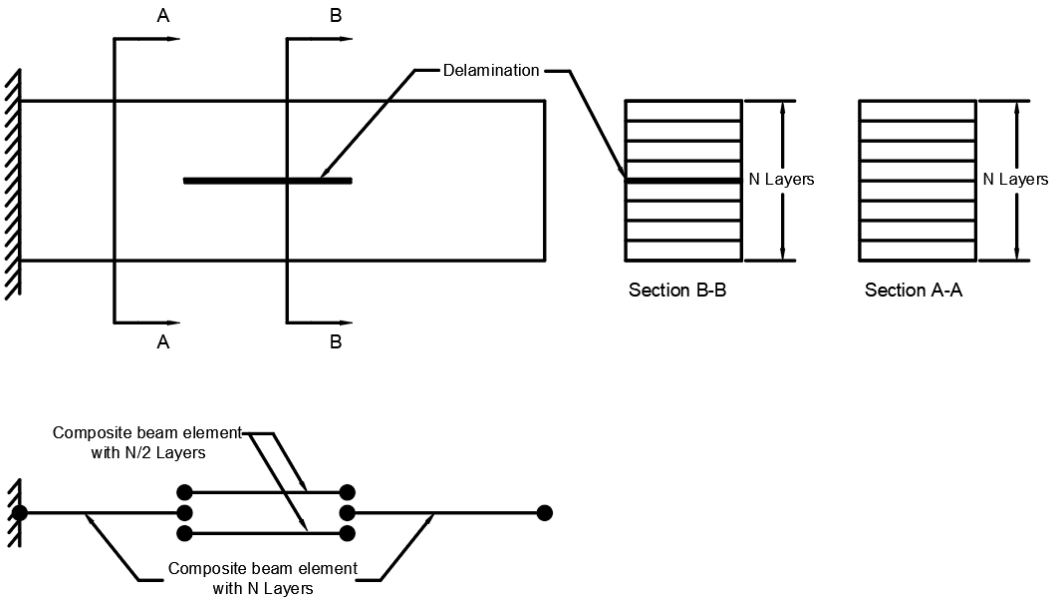

Figure 1.1: Modeling assumption for delaminated composite beam

1.3. Objective of the thesis

The global objective of this work is to propose a computationally efficient model for dynamic analysis of isotropic beams and laminated composite beams and show the application of this model in vibration-based damage detection. To achieve this objective, the following steps were taken:

1) Adopt a spectral finite element model for dynamic analysis of isotropic beams and laminated composite beams.

2) Consider both the transient and the steady-state response obtained by spectral finite element method and adopt a method to calculate the transient response based on the steady-state response.

3) Extract the free vibration features, natural frequencies and mode shapes, directly from the frequency-dependent stiffness matrix.

4) Propose a spectral finite element model for dynamic analysis of delaminated composite beams.

5) Verify the obtained results by comparing the output of the proposed model with numerical and experimental results from previous works.

6) Develop a vibration-based damage detection program based on the developed dynamic analysis model to detect location and severity of damage in damaged isotropic beams and to detect delamination location and size in delaminated composite beams using natural frequencies and vibration mode shapes.

1.4. Layout of the thesis

This thesis is organized into 5 chapters:

Chapter 1 covers the motivation, scope and objective of the thesis.

Chapter 2 gives a brief literature review on the previous works on dynamic analysis of laminated composite beams, spectral finite element method, free-vibration analysis using the frequency-based dynamic stiffness matrix, vibration-based damage detection techniques and application of Genetic Algorithm as an optimization tool in damage detection problems.

Chapter 3 contains the methodology of the thesis and covers a large portion of the thesis. A Spectral finite element model for vibration of beam element is introduced. A discussion is given on the output response of the spectral finite element model and a method is suggested to add the free vibration response. Wittrick-Williams method is combined with bisection method to search for natural frequencies of vibration. A vibration-based damage detection method is developed and genetic algorithm is used as the optimization tool. The entire process is repeated for laminated composite beams. A spectral finite element model is proposed for laminated composite beams and laminated composite beams with delamination. Natural frequencies are calculated using Wittrick-Williams method. A model is introduced to consider the effect of distributed contact between the delaminated top and bottom surfaces. The damage detection algorithm is applied to the analysis tool to detect location and length of delamination in delaminated composite beams.

Chapter 4 includes the case studies. Natural frequencies and mode shapes of isotropic beams are calculated using the spectral finite element model and the program results are validated by comparing with the analytical results. The results are also obtained by conventional finite element models and the effect of mesh refinement on the performance of the conventional finite element model is discussed. Total response of a beam under different load functions are built using the proposed transient method and the results are compared with the analytical solution. Natural frequencies of symmetric laminated composite beams with and without midplane delamination are obtained using the spectral finite element model and compared with results from previous works. The effect of delamination location on natural frequencies of different modes of vibration is studied

and it is shown that delamination effects are more significant on higher modes of vibration. The performance of the damage detection algorithm is shown with both damaged isotropic beams and delaminated composite beams.

Chapter 5 concludes the thesis and summarizes its achievements. It also provides suggestions for future works that can be done based on this thesis.

Chapter 2

Literature Review

2.1. Use of Composites

Composite structures have become the most popular choice in structural engineering during recent years. They offer an advantage for structures which require a combination of high strength and low weight. In contrast to their in-plane properties, transverse tensile and inter laminar shear strength of laminated composite beams are quite low. Consequently, laminated composite beams are susceptible to delamination from a wide variety of sources which includes fabrication stresses, environmental cycling, handling damage and foreign object impact damage [Pardoen and Tracy, 1988]. Delamination not only affects the strength and integrity of the structure by contributing to its final failure, but also causes a reduction in the stiffness, thus affecting its vibrational and stability characteristics [Majmudar and Suryanarayan, 1988].

2.2. Damage detection techniques

Non-destructive testing (NDT) such as thermography and ultrasonic inspection have become common in damage detection in composite beams. However, they cannot be used for real time damage detection. [Ihesiulor et al, 2013] A recent development in health monitoring of structures is vibration-based damage detection. Structural damage usually decreases the structural stiffness which produces changes in the vibration characteristics of the structure. The usual vibration-based damage identification system includes two main modules:

1. A simulation module that finds the vibration properties of trial models such as the natural frequencies and mode shapes
2. A search module including an optimization algorithm that tries to find the closest model to the target vibration features.

The implemented algorithm must satisfy the levels of Structural Health Monitoring depending on the expected application. These levels are:

Level 1: Finding out the possibility of damage. Essentially this means that the SHM system should be able to confirm if damage is present in the structural system

Level 2: Estimation of damage location and size

Level 3: Estimation the severity of damage [Garg et al, 2004]

Level 4: Updating the Finite Element model of the structure for further analysis

Modal testing is one of the techniques for studying the behavior of a structure through a number of natural frequencies and mode shapes [Bagchi, 2005]. The use of dynamic testing to detect and quantify the effect of internal damage on modal parameters has become a popular research area. [Vandiver 1975, 1977] examined the change in the frequencies associated with the first two bending modes and first torsional mode of an offshore light station tower to identify damage. [Cawley and Adams, 1979] gave a formulation to detect damage in composite materials from frequency shifts. [Penny, et al. 1993] presented a method for locating the most likely damage case by simulating the frequency shifts that would occur for all damage cases under consideration. [Mottershead and Friswell, 1993] gave a survey of model updating methods that can be used as damage detection procedures.

Fatigue cracking and delamination are particularly dangerous and are at the same time the most common kind of damage in elements of machines and structures. It is of great importance for their safety operation to ensure that the elements of machines and structures are free of any fatigue cracks and delamination and in the case of their presence to determine their extent [Ostachowicz, 2007]. One example is investigating the effect of damage after impulse impact on dynamic properties of composite laminates. Comparison of modal parameters before and after impact shows that the frequency reduction predominantly appears in higher modes [Pardoen, 1988]. This observation shows the importance of an analysis tool that can calculate higher modes of vibration in an efficient way.

2.3. Spectral Finite Element Method

Structural modeling is usually carried out using the finite element method. However, finite element method produces fair estimation of natural frequencies only at the lower part of the frequency spectrum. One can expect from a discrete model of order n to produce fewer than $\frac{n}{3}$ eigenvalues with reasonable accuracy [Kumar and Yitshak, 2002]. The reason is that the conventional finite element treats the distributed load induced by the mass as concentrated load applied at the ends of the element. Therefore, many elements must be used if the mass distribution is to be modeled

accurately [Doyle, 1990]. [Doyle, 1990] formulated a bar and a beam spectral element which treated the distributed mass exactly. Only one spectral beam element needs to be placed between any two joints and this decreases the number of degrees of freedom of the system.

2.4. Free vibration analysis

Spectral element formulation results in a transcendental eigenvalue problem when it comes to free vibration analysis. The dynamic stiffness matrix is no longer a linear function of ω^2[Wittrick and Williams, 1970]. [Kumar and Yitshak, 2002] used Newton's eigenvalue iteration method to solve the eigenvalue problem. Their proposed method requires deriving the derivative of the dynamic stiffness matrix with respect to ω which could be problematic in cases where complicated and long terms appear in the dynamic stiffness matrix.

A method based on counting the number of natural frequencies exceeded by any arbitrary value for ω is suggested by [Wittrick , 1970]. The Wittrick-Williams method relies on having access to the number of frequencies of a clamped-clamped element that are less than a trial value called J_0 and the dynamic stiffness matrix of the system.

2.5. Calculation of the forced vibration response

According to [Doyle, 1997], the forced vibration response should be calculated by transforming the force function to frequency domain using Fourier Transform. After calculating the response in frequency domain using SFEM, the response should be reconstructed in time domain using Inverse Fourier Transform. The response calculated by SFEM is the steady-state part of the response which does not contain the free vibration part of the solution. [Cho and Lee, 2007] used a pseudo force method to add the transient response due to non-null initial conditions. However, it seems that the proposed method is unable to incorporate the transient part when initial conditions are zero. [Veletsos and Kumar, 1983] proposes an approach to calculate the transient response using initial conditions and the steady-state response of a single degree of freedom system and extends it to multi-degree of freedom systems if vibration mode shapes and mass matrix of the system are available.

2.6. Genetic algorithm

[Moller and Friberg, 1998] introduced an objective function that represents to what extent a particular trial structure agrees with experimental results. [Xinjun and Yang, 2018] used two

optimization algorithms, the Levenberg_Maquardt and the trust region reflective algorithms, to update the FE model of a concrete building frame. The FE model was built in SAP 2000 using conventional finite element. They indicated that it is possible that the cost function is non-convex, so in general the global optimality of the optimization results cannot be guaranteed. [Hao and Yang, 2002] used the genetic algorithm to update the FE model of a cantilever beam. Genetic Algorithm searches from a population of points in the region of the whole solution space. They also used the conventional finite element as the simulator. [Lee and Shin, 2001] built a spectral finite element damage detection procedure and compared the results with the results of a tool that used finite element. They showed that due to exactness of shape functions used in spectral finite element models, they perform better in locating small damage. [Nag et al, 2002] built a delamination detection tool that implements GA to minimize the objective function. One objective function was based on displacement and the other was based on power.

Chapter 3

Methodology

3.1. Differential equation of motion of a bar [Clough and Penzien, 1995]

Consider a straight bar for which the axial stiffness is EA and mass per unit length is constant and equal to m, and $u(x,t)$ is the axial displacement. If it is subjected to an arbitrary external distributed axial loading $q(x,t)$, an internal time-varying axial-force distribution $N(x,t)$ will be produced. Forces acting on a differential segment of the bar are shown in Figure 3.1:

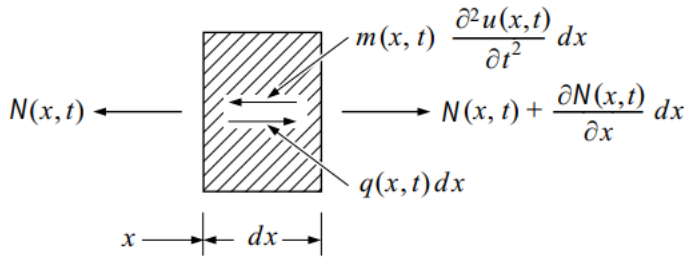

Figure 3.1 : Differential bar element [Clough and Penzien, 1995]

Summing the forces in the x direction gives:

$$N(x,t) + f_I(x,t)dx - \left[N(x,t) + \frac{\partial N(x,t)}{\partial x}dx\right] = q(x,t)\mathrm{dx} \tag{3.1}$$

$f_I(x,t)$ is the inertial force which is:

$$f_I(x,t) = m\frac{\partial^2 u(x,t)}{\partial t^2} \tag{3.2}$$

The axial force-displacement relationship is written as:

$$N(x,t) = EA\frac{\partial u(x,t)}{\partial x} \tag{3.3}$$

Substituting Eq 3.3 in Eq. 3.1, the partial differential equation of motion of an axial bar is obtained as:

$$m\frac{\partial^2 u(x,t)}{\partial t^2} - EA\frac{\partial^2 u(x,t)}{\partial x^2} = q(x,t) \tag{3.4}$$

In the case of free vibration, external forces are assumed to be zero and the partial differential equation will be:

$$m\frac{\partial^2 u(x,t)}{\partial t^2} - EA\frac{\partial^2 u(x,t)}{\partial x^2} = 0 \tag{3.5}$$

3.2. Spectral element formulation [Doyle, 1988]

Eq. 3.5 can be rewritten as:

$$\frac{\partial^2 u(x,t)}{\partial t^2} - k^2\frac{\partial^2 u(x,t)}{\partial x^2} = 0\,, k = \sqrt{\frac{EA}{m}} \tag{3.6}$$

In which k is the wave speed, E is the modulus of elasticity, A is the area of the cross-section and m is mass per unit length and is assumed to be constant. It is known that the solution of the wave equation in Eq 3.6 is in the form given in Eq 3.7:

$$u(x,t) = \phi(x)e^{i\omega t} \tag{3.7}$$

where ω is the angular frequency and the amplitude $\phi(x)$ satisfies the following equation:

$$-\frac{d^2\phi(x)}{dx^2} - a^2\phi(x) = 0 \tag{3.8}$$

where a^2 appears as a separation constant and indeed $a = \frac{\omega}{k}$ is the wave number and its relation to frequency is called the spectrum relation. As for the spectral finite element one can solve this wave equation analytically. This has the simple solution:

$$\phi(x) = Ae^{-iax} + Be^{iax} \tag{3.9}$$

In finite element terms this is called the shape function, but obviously in this case it is dependent on the frequency ω and it is different at each frequency. Using subscripts 1 and 2, $\phi_1 = \phi(0)$ and $\phi_2 = \phi(L)$ for the nodal displacements, the coefficients A and B can be related to the nodal displacements as:

$$\begin{Bmatrix} A \\ B \end{Bmatrix} = \frac{1}{(1-e^{-i2aL})}\begin{bmatrix} 1 & -e^{-iaL} \\ -e^{-iaL} & 1 \end{bmatrix}\begin{Bmatrix} \phi_1 \\ \phi_2 \end{Bmatrix} \tag{3.10}$$

The forces can be determined by differentiation of the displacement, i.e. $N(x,t) = EA\frac{\partial u(x,t)}{\partial x}$ .By using that $N(x,t) = N(x)e^{i\omega t}$, one obtains:

$$\begin{Bmatrix} N_1 \\ N_2 \end{Bmatrix} = \frac{EA}{L}\frac{ial}{(1-e^{-i2aL})}\begin{bmatrix} 1+e^{-i2aL} & -2e^{-iaL} \\ -2e^{-iaL} & 1+e^{-i2aL} \end{bmatrix}\begin{Bmatrix} \phi_1 \\ \phi_2 \end{Bmatrix} \tag{3.11}$$

where $N_1 = N(0)$ and $N_2 = N(L)$ was introduced. The above relation can be written alternatively as:

$$\begin{Bmatrix} N_1 \\ N_2 \end{Bmatrix} = \frac{EA}{L}\frac{aL}{\sin(aL)}\begin{bmatrix} \cos(aL) & -1 \\ -1 & \cos(aL) \end{bmatrix}\begin{Bmatrix} \phi_1 \\ \phi_2 \end{Bmatrix} \tag{3.12}$$

The above relation can be written in the familiar form $\{\boldsymbol{f}\} = [\boldsymbol{k}]\{\boldsymbol{\phi}\}$, where $[\boldsymbol{k}]$ is the frequency dependent dynamic element stiffness of the bar. If $\{\boldsymbol{\phi}\}$ is solved, $\phi(x)$ is obtained in terms of nodal values $\phi_1$and ϕ_2 as shown in Eq 3.13.

$$\phi(x) = \frac{\sin\big(a(L-x)\big)}{\sin(aL)}\phi_1 + \frac{\sin(ax)}{\sin(aL)}\phi_2 \tag{3.13}$$

3.3. Differential equation of motion of an Euler-Bernoulli beam [Clough and Penzien, 1995]

The equation of motion of an Euler Bernoulli beam element can be derived by considering the equilibrium of forces for a differential segment of the beam. $v(x,t)$ is the transverse displacement of the beam, EI is the flexural stiffness and assumed to be constant and m is mass per unit length. No shear deformation is considered in this formulation. $V(x,t)$ is the vertical force acting on the cut section. $p(x,t)$ is the transverse loading and is assumed to vary with position and time.

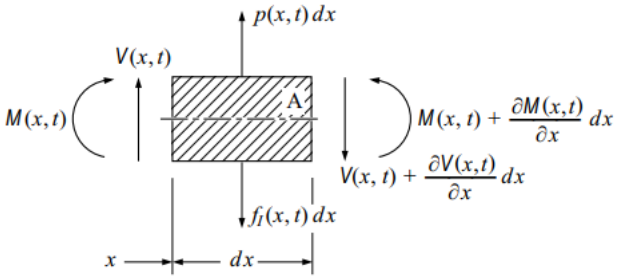

Figure 3.2: Differential beam element [Clough and Penzien, 1995]

Summing all the forces acting vertically leads to:

$$V(x,t) + p(x,t)\,dx - \left[\,V(x,t) + \frac{\partial V(x,t)}{\partial x}dx\,\right] - f_I(x,t)dx = 0 \tag{3.14}$$

$f_I(x,t)$dx is the resultant transverse inertial force equal to the mass of the element multiplied by its transverse acceleration:

$$f_I(x,t) = m\,\frac{\partial^2 v(x,t)}{\partial t^2} \tag{3.15}$$

Eq. 3.14 can be rewritten as:

$$\frac{\partial V(x,t)}{\partial x} = p(x,t) - m\frac{\partial^2 v(x,t)}{\partial t^2} \tag{3.16}$$

The moment equilibrium equation for the differential element is written as:

$$M(x,t) + V(x,t)dx - \left[M(x,t) + \frac{\partial M(x,t)}{\partial x}dx\right] = 0 \tag{3.17}$$

The above equilibrium relationship is obtained by summing moments about point A on the elastic axis after dropping the two second-order moment terms involving the inertia and applied loadings, one gets:

$$V(x,t) = \frac{\partial M(x,t)}{\partial x} \tag{3.18}$$

Differentiating Eq. 3.18 with respect to x and substituting in Eq. 3.16 gives:

$$\frac{\partial^2 M(x,t)}{\partial x^2} + m\frac{\partial^2 M(x,t)}{\partial t^2} = p(x,t) \tag{3.19}$$

It is known that the moment can be written as Eq. 3.20:

$$M = EI\frac{\partial^2 v}{\partial x^2} \tag{3.20}$$

So, Eq. 3.19 becomes Eq. 3.21:

$$EI\frac{\partial^4 v(x,t)}{\partial x^4} + m\frac{\partial^2 v(x,t)}{\partial t^2} = p(x,t) \tag{3.21}$$

In the case of free vibration, external forces are assumed to be zero and the partial differential equation will be:

$$EI\frac{\partial^4 v(x,t)}{\partial x^4} + m\frac{\partial^2 v(x,t)}{\partial t^2} = 0 \tag{3.22}$$

Transverse displacement is a function of x and t and is written as the product of a temporal function and a spatial function as:

$$v(x,t) = X(x)T(t) \tag{3.23}$$

This indicates that the motion is of a specific shape $X(x)$ and having a time dependent amplitude $T(t)$. Substituting Eq 3.23 into 3.24 gives:

$$X^{(4)}(x)T(t) + \frac{m}{EI}\ddot{T}(t)X(x) = 0 \tag{3.24}$$

$\ddot{T}\ (t)$ is the second derivative of $T(t)$ with respect to t and $X^{(4)}(x)$ is the fourth derivative of $X(x)$ with respect to x. Dividing Eq. 3.24 by $X(x)T(t)$, the above equation is rewritten as:

$$\frac{X^{(4)}(x)}{X(x)} + \frac{m}{EI}\frac{\ddot{T}(t)}{T(t)} = 0 \tag{3.25}$$

Because the first term in this equation is a function of x only and the second term is a function of t only, the entire equation can be satisfied for arbitrary values of x and t only if each term is a constant:

$$EI\frac{X^{(4)}(x)}{X(x)} = -\mathrm{m}\frac{\ddot{T}(t)}{T(t)} = c \tag{3.26}$$

where:

$$EI\frac{X^{(4)}(x)}{X(x)} = c \tag{3.27}$$

and:

$$-m\frac{\ddot{T}\ (t)}{T(t)} = c \tag{3.28}$$

Both temporal and spatial functions are assumed to have a harmonic shape as in Eq. 3.29 and Eq. 3.30:

$$T(t) = \ \bar{B}e^{i\omega t} \tag{3.29}$$

and

$$X(x) = \bar{C}e^{i\alpha x} \tag{3.30}$$

Applying Eq 3.29 into Eq 3.28 gives:

$$-m\frac{\bar{B}\ \omega^2 e^{i\omega t}}{\bar{B}\ e^{i\omega t}} = c \tag{3.31}$$

The constant c is calculated from the above equations as:

$$c = \ -m\omega^2 \tag{3.32}$$

Similarly, if Eq. 3.30 is substituted in Eq. 3.27:

$$EI\frac{\bar{C}\alpha^4 e^{i\alpha x}}{\bar{C}e^{i\alpha x}} = c \tag{3.33}$$

Simplifying the above equation gives:

$$c = EI\alpha^4 \tag{3.34}$$

Setting the right-hand side of Eq 3.34 equal to left-hand side of Eq. 3.33 gives Eq. 3.35:

$$EI\alpha^4 + m\omega^2 = 0 \tag{3.35}$$

Eq. 3.35 is called the characteristic equation. Solutions to this equation are wave numbers. Wave numbers determine the deformation of the beam element at any given frequency, ω which are:

$$\alpha_1 = \sqrt[4]{\frac{m\omega^2}{EI}}, \alpha_2 = i\sqrt[4]{\frac{m\omega^2}{EI}}, \alpha_3 = -\sqrt[4]{\frac{m\omega^2}{EI}}, \alpha_4 = -i\sqrt[4]{\frac{m\omega^2}{EI}} \tag{3.36}$$

The spatial part of the solution is written as the linear combination of the spatial waves shown in Eq. 3.37:

$$X(x) = Ae^{i\alpha_1 x} + Be^{i\alpha_2 x} + Ce^{i\alpha_3 x} + De^{i\alpha_4 x} \tag{3.37}$$

The entire solution is written in Eq. 3.38 and Eq. 3.39:

$$v(x,t) = \left(Ae^{i\alpha_1 x} + Be^{i\alpha_2 x} + Ce^{i\alpha_3 x} + De^{i\alpha_4 x}\right)e^{i\omega t} \tag{3.38}$$

and

$$\theta(x,t) = \left(Ai\alpha_1 e^{i\alpha_1 x} + Bi\alpha_2 e^{i\alpha_2 x} + Ci\alpha_3 e^{i\alpha_3 x} + Di\alpha_4 e^{i\alpha_4 x}\right)e^{i\omega t} \tag{3.39}$$

3.4. Development of the spectral beam element [Black, 2005]

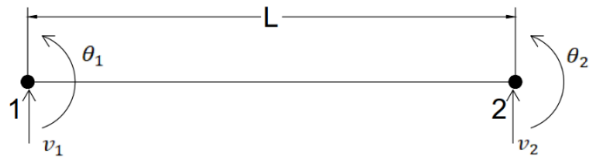

Figure 3.3: Degrees of freedom in the finite beam element

Figure 3.3 shows an Euler-Bernoulli beam element with 2 degrees of freedom on each node, a rotational degree of freedom shown with θ and a transverse degree of freedom shown with v. L is the length of the beam element. The nodal degrees of freedom are assumed to have a harmonic shape as shown in Eq. 3.40 below:

$$\{\boldsymbol{d}\} = \begin{bmatrix} v(0,t) \\ \theta(0,t) \\ v(l,t) \\ \theta(l,t) \end{bmatrix} = \begin{bmatrix} v_1 \\ \theta_1 \\ v_2 \\ \theta_2 \end{bmatrix} e^{i\omega t} \tag{3.40}$$

One can rewrite the vector $\begin{bmatrix} v_1 \\ \theta_1 \\ v_2 \\ \theta_2 \end{bmatrix}$ in terms of vector $\begin{bmatrix} A \\ B \\ C \\ D \end{bmatrix}$ using Eq. 3.38 and Eq. 3.39:

$$\begin{bmatrix} v(0,t) \\ \theta(0,t) \\ v(l,t) \\ \theta(l,t) \end{bmatrix} = \begin{bmatrix} 1 & 1 & 1 & 1 \\ i\alpha_1 & i\alpha_2 & i\alpha_3 & i\alpha_4 \\ e^{i\alpha_1} & e^{i\alpha_2} & e^{i\alpha_3} & e^{i4} \\ i\alpha_1 e^{i\alpha_1} & i\alpha_2 e^{i\alpha_2} & i\alpha_3 e^{i3} & i\alpha_4 e^{i\alpha_4} \end{bmatrix} \begin{bmatrix} A \\ B \\ C \\ D \end{bmatrix} e^{i\omega t} = [\boldsymbol{D}] \begin{bmatrix} A \\ B \\ C \\ D \end{bmatrix} e^{i\omega t} \tag{3.41}$$

where $[\boldsymbol{D}]$ is:

$$[\boldsymbol{D}] = \begin{bmatrix} 1 & 1 & 1 & 1 \\ i\alpha_1 & i\alpha_2 & i\alpha_3 & i\alpha_4 \\ e^{i\alpha_1} & e^{i\alpha_2} & e^{i\alpha_3} & e^{i4} \\ i\alpha_1 e^{i\alpha_1} & i\alpha_2 e^{i\alpha_2} & i\alpha_3 e^{i3} & i\alpha_4 e^{i\alpha_4} \end{bmatrix} \tag{3.42}$$

Moment and shear force are written at the nodes using Eq. 3.18 and Eq. 3.20:

$$\begin{bmatrix} V(0,t) \\ -M(0,t) \\ -V(l,t) \\ M(l,t) \end{bmatrix} = \begin{bmatrix} V_1 \\ M_1 \\ V_2 \\ M_2 \end{bmatrix} e^{i\omega t} \tag{3.43}$$

$$= EI \begin{bmatrix} -i\alpha_1^3 & -i\alpha_2^3 & -i\alpha_3^3 & -i\alpha_4^3 \\ \alpha_1^2 & \alpha_2^2 & \alpha_3^2 & \alpha_4^2 \\ i\alpha_1^3 e^{i\alpha_1 L} & i\alpha_2^3 e^{i\alpha_2 L} & i\alpha_3^3 e^{i\alpha_3 L} & i\alpha_4^3 e^{i\alpha_4 L} \\ -\alpha_1^2 e^{i\alpha_1 L} & -\alpha_2^2 e^{i\alpha_2 L} & -\alpha_3^2 e^{i\alpha_3 L} & -\alpha_4^2 e^{i\alpha_4 L} \end{bmatrix} \begin{bmatrix} A \\ B \\ C \\ D \end{bmatrix} e^{i\omega t}$$

$$= [\boldsymbol{R}] \begin{bmatrix} A \\ B \\ C \\ D \end{bmatrix} e^{i\omega t}$$

where $[\boldsymbol{R}]$ is equal to:

$$[\boldsymbol{R}] = EI \begin{bmatrix} -i\alpha_1^3 & -i\alpha_2^3 & -i\alpha_3^3 & -i\alpha_4^3 \\ \alpha_1^2 & \alpha_2^2 & \alpha_3^2 & \alpha_4^2 \\ i\alpha_1^3 e^{i\alpha_1 L} & i\alpha_2^3 e^{i\alpha_2 L} & i\alpha_3^3 e^{i\alpha_3 L} & i\alpha_4^3 e^{i\alpha_4 L} \\ -\alpha_1^2 e^{i\alpha_1 L} & -\alpha_2^2 e^{i\alpha_2 L} & -\alpha_3^2 e^{i\alpha_3 L} & -\alpha_4^2 e^{i\alpha_4 L} \end{bmatrix} \tag{3.44}$$

The nodal forces are expressed with vector $\{\mathbf{f}\}$ as:

$$\{\boldsymbol{f}\} = \begin{bmatrix} V_1 \\ M_1 \\ V_2 \\ M_2 \end{bmatrix} e^{i\omega t} \tag{3.45}$$

Nodal forces can be related to the nodal displacements with $\left[\boldsymbol{K}_{dyn}\right]$ as:

$$\{\boldsymbol{f}\} = \left[\boldsymbol{K}_{dyn}\right]\{\boldsymbol{d}\} \tag{3.46}$$

where $\left[\boldsymbol{K}_{dyn}\right]$is equal to:

$$[\boldsymbol{K}(\omega)] = [\boldsymbol{R}][\boldsymbol{D}]^{-1} \tag{3.47}$$

3.5. Fourier transform:

It has long been known that an arbitrary signal can be thought of as the superposition of many sinusoidal components, that is, it has a distribution or spectrum of components. Working in terms of the spectrum is called a spectral analysis. [Doyle, 1997]. A Function in frequency domain is shown by a continuous distribution of components which is known as its continuous Fourier transform (CFT). The transform and its inverse are shown in Eq. 3.48 and Eq. 3.49.

$$\hat{C}(\omega) = \int_{-\infty}^{\infty} F(t) e^{-i\omega t} dt \tag{3.48}$$

$$F(t) = \int_{-\infty}^{\infty} \hat{C}(\omega) e^{i\omega t} d\omega \tag{3.49}$$

In the equations above $F(t)$ could be any function in time domain. It should be noted that continuous transforms are feasible only if the function to be transformed is mathematically simple. Applications of the frequency-domain analysis procedure therefore is limited to cases for which the Fourier integral transforms of the applied loading functions are available, and even in these cases the evaluation of the integrals can be a tedious process. To make the procedure practical, it is necessary to formulate the procedure by using a numerical analysis approach.

The function $F(t)$ for one period is divided into N_0 piecewise-constant segments whose heights are F_m and base are $\Delta T = \frac{\mathrm{T}}{\mathrm{N}_0}$, where T is the period of the function. It is important to select the sampling time window such that it exactly matches the period of the signal. We can regard each rectangle under the curve in Figure 3.4 as an impulse having the area $F_m \Delta T$.

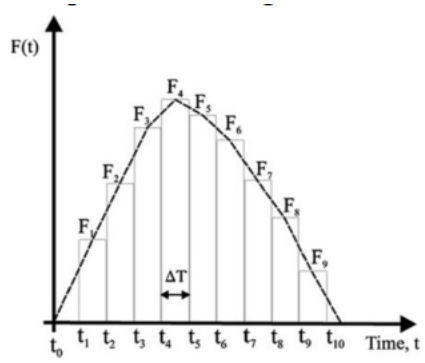

Figure 3.4: Function in time domain

Function $\hat{C}(\omega)$ is evaluated at N_0 points and shown with coefficients C_n which are obtained from:

$$C_n = \frac{\Delta T}{T}\sum_{m=0}^{N-1} F_m e^{-i\frac{2\pi nm}{N}} \tag{3.50}$$

The coefficients in the matrix form can be written as:

$$\begin{Bmatrix} C_0 \\ C_1 \\ C_2 \\ . \\ . \\ . \\ C_{N-1} \end{Bmatrix} = \frac{1}{N}\begin{bmatrix} 1 & 1 & 1 & 1 & \dots & 1 \\ 1 & W & W^2 & W^3 & \dots & W^{N-1} \\ 1 & W^2 & W^4 & W^6 & \dots & W^{2(N-1)} \\ : & : & : & : & : & : \\ 1 & W^{N-1} & W^{2(N-1)} & W^{3(N-1)} & \dots & W^{(N-1)(N-1)} \end{bmatrix} \begin{Bmatrix} F_0 \\ F_1 \\ F_2 \\ . \\ . \\ . \\ F_{N-1} \end{Bmatrix} \tag{3.51}$$

where $W^{nm} = e^{-i\frac{2\pi nm}{N}}$. The matrix of exponents that contains all the values for $-i\frac{2\pi nm}{N}$ when $n = 0,1,2,\dots,N_0 - 1$ and $m = 0,1,2,\dots,N_0 - 1$ can be written as:

$$-i\frac{2\pi}{N}\begin{bmatrix} 0 & 0 & 0 & 0 & \dots & 0 \\ 0 & 1 & 2 & 3 & \dots & N-1 \\ 0 & 2 & 4 & 6 & \dots & 2(N-1) \\ : & : & : & : & : & : \\ 0 & N-1 & 2(N-1) & 3(N-1) & \dots & (N-1)(N-1) \end{bmatrix}$$

When the time function is real, C_0 is obtained as real without a complex counterpart and the pairs (C_{N-n}, C_n) and (C_{-n}, C_n) are complex conjugates. In structural wave propagation analyses the excitation signal is real. As the consequence of the input signal being real-only, the DFT of the

time-signal is also symmetric about the origin as well as Nyquist frequency. The transform beyond the Nyquist frequency is the complex conjugate of the transform before this frequency. What this means is that N real points of the time-signal are transformed into $N/2$ complex points in the frequency domain and no information is gained or lost because the complex points contain double information compared to real points. Useful frequency range is thus half of the final frequency. Knowing the sampling rate ΔT , Nyquist frequency is given by:

$$f_{Nyquist} = \frac{1}{2\Delta T} \tag{3.52}$$

Using the discrete transforms puts an upper limit on the maximum frequency available to characterize the signal. Nyquist frequency increases only when ΔT decreases. Thus, for a fixed number of points, fine resolution in the time domain (small ΔT) means course resolution in the frequency domain (large Δω). Finer resolution in the frequency domain is achieved only by increasing the sample length. For Discrete Fourier Transforms the largest significant frequency in the signal should be less than the Nyquist frequency.

Fast Fourier Transform

A straightforward evaluation of C_n would require N^2 complex multiplications. However, it is easy to realize that in Discrete Fourier Transform same values of W_N^{nm} are used many times. Firstly, the product $n \times m$ repeats for different values of n and m. Secondly, W_N^{nm} is a periodic function with only N distinct values. We see that many of the computations used in forming one of the summations is also used in the others. The re-use of the same computations is the reason a great reduction of computational effort is afforded by the FFT. The number of computations with and without the FFT algorithm are given by $\frac{3}{2} N \log_2 N$ and $2N^2$. [Doyle, 1997]

3.6. Conventional Euler-Bernoulli beam Finite Element [Reddy, 1989]

The governing differential equation that is solved using the conventional finite element method is shown below:

$$EIv^{iv} = 0 \tag{3.53}$$

v^{iv} shows the fourth derivative of v with respect to x. If the interpolation functions can generate the homogenous solution of the differential equilibrium equation, then the finite element solution using these interpolation functions in the total potential energy expression provides exact nodal displacements. For Euler-Bernoulli beam the homogenous solution of $EIv^{iv} = 0$ is obtained as:

$$v = dx^3 + cx^2 + bx + a \tag{3.54}$$

As Finite Element solution is a special form of the minimum total potential energy solution (Ritz solution), a finite element solution can be developed using the trial function in Eq. 3.54 by satisfying the interelement continuity of the displacement field. For this purpose, at the element ends the displacements are specified to be the nodal displacements, i.e.

$$v(0) = v_1, v'(0) = \theta_1, v(L) = v_2, v'(L) = \theta_2 \tag{3.55}$$

In the equation above, $v'$is the first derivative of v with respect to x.

What is denoted in Eq 3.55, can be written in the vectorial form as:

$$\begin{bmatrix} v_1 \\ \theta_1 \\ v_2 \\ \theta_2 \end{bmatrix} = \begin{bmatrix} 0 & 0 & 0 & 1 \\ 0 & 0 & 1 & 0 \\ L^3 & L^2 & L & 1 \\ 3L^2 & 2L & 1 & 0 \end{bmatrix} \begin{bmatrix} d \\ c \\ b \\ a \end{bmatrix} \tag{3.56}$$

The displacement interpolation function for an element can be written as:

$$v = [x^3 \quad x^2 \quad x \quad 1] \begin{bmatrix} 0 & 0 & 0 & 1 \\ 0 & 0 & 1 & 0 \\ L^3 & L^2 & L & 1 \\ 3L^2 & 2L & 1 & 0 \end{bmatrix}^{-1} \begin{bmatrix} v_1 \\ \theta_1 \\ v_2 \\ \theta_2 \end{bmatrix} = [H_1 \quad H_2 \quad H_3 \quad H_4] \begin{bmatrix} v_1 \\ \theta_1 \\ v_2 \\ \theta_2 \end{bmatrix} \tag{3.57}$$

$$= [\boldsymbol{H}]\{\boldsymbol{d}_e\}$$

where:

$$H_1 = 1 - \frac{3x^2}{L^2} + \frac{2x^3}{L^3} \tag{3.58}$$

$$H_2 = x - \frac{2x^2}{L} + \frac{x^3}{L^2} \tag{3.59}$$

$$H_3 = \frac{3x^2}{L^2} - \frac{2x^3}{L^3} \tag{3.60}$$

$$H_4 = -\frac{x^2}{L} + \frac{x^3}{L^2} \tag{3.61}$$

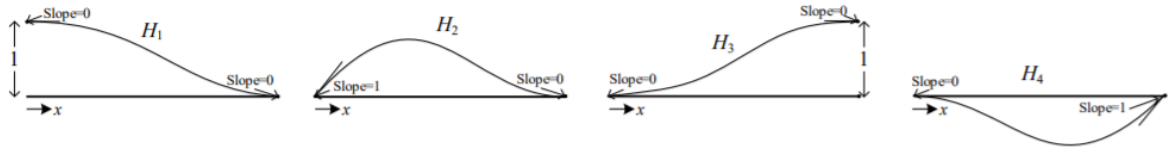

Figure 3.5: Conventional beam shape functions

Minimizing the total potential energy is adopted to calculate the stiffness matrix of the beam. The minimum of total potential energy principle states that in a conservative system, among all kinematically possible configurations of the system the one that satisfies the equilibrium makes the total potential energy a minimum. The total potential energy Π is the internal strain energy stored during deformation U plus the external potential of the applied load W_{ext} that is shown in the equation below:

$$\Pi = U + W_{ext} \tag{3.62}$$

Total potential energy is a function of the deformed configuration (i.e. displacement function). Thus, it is a function of functions which is called a functional. A functional is a scalar quantity depending on some function or several functions. The functional can be treated as a function of an infinite number of independent variables.

The minimum principle states that $\Pi(\mathrm{w}, \mathrm{w}', \mathrm{w}'', \dots) \leq \Pi(\bar{\mathrm{w}}, \bar{\mathrm{w}}', \bar{\mathrm{w}}'', \dots)$, where w is the true displacement field and $\bar{\mathrm{w}}$ is any kinematically admissible displacement field. Like the minimum of functions, the minimum of potential energy occurs where the derivative (called variation) of the potential energy vanishes:

$$\delta\Pi = 0 \tag{3.63}$$

Assuming that the potential energy is a function of displacement w, its variation can be written as:

$$\delta\Pi = \frac{\partial \Pi}{\partial w}\delta w \tag{3.64}$$

Assuming $\delta w \neq 0$, Eq. 3.63 becomes:

$$\frac{\partial \Pi}{\partial w} = 0 \tag{3.65}$$

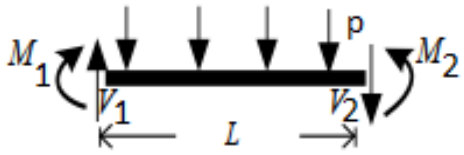

Figure 3.6: Forces applied on a beam element

For Euler-Bernoulli beam element with the length of L shown in Figure 3.6 where M_1 and M_2 are the nodal moments and V_1 and V_2 are the nodal shear forces and p is the distributed external load, the total potential energy can be written as:

$$\Pi(\mathrm{v}) = \frac{1}{2}\int_0^L EI\left(\frac{d^2v}{dx^2}\right)dx + \int_0^L pvdx - V_1 v\,\big|_{x=0} + V_2 v\,\big|_{x=L} - M_1 v'\,\big|_{x=0} + M_2 v'\,\big|_{x=L} \tag{3.66}$$

By substituting the interpolation functions (Eq. 3.58-3.61) into the first term on the right-hand-side of Eq. 3.66 (strain energy term in the total potential energy), the stiffness matrix of the finite element can be developed as:

$$U = \frac{1}{2}\int_0^L EI\left(\frac{d^2v}{dx^2}\right)dx = \frac{1}{2}EI\{\boldsymbol{d}_e\}^T\int_0^L\left[\frac{d^2\boldsymbol{H}}{dx^2}\right]^T\left[\frac{d^2\boldsymbol{H}}{dx^2}\right]dx\,\{\boldsymbol{d}_e\} = \frac{1}{2}\{\boldsymbol{d}_e\}^T[\boldsymbol{K_e}]\{\boldsymbol{d}_e\} \Rightarrow \tag{3.67}$$

$$\delta U = \{\delta\boldsymbol{d}_e\}^T[\boldsymbol{K_e}]\{\boldsymbol{d}_e\}$$

where:

$$[\boldsymbol{K_e}] = EI \int_0^L \left[\frac{d^2\boldsymbol{H}}{dx^2}\right]^T \left[\frac{d^2\boldsymbol{H}}{dx^2}\right] dx \tag{3.68}$$

$$= EI \int_0^L \begin{bmatrix} \frac{d^2H_1}{dx^2}\frac{d^2H_1}{dx^2} & \frac{d^2H_1}{dx^2}\frac{d^2H_2}{dx^2} & \frac{d^2H_1}{dx^2}\frac{d^2H_3}{dx^2} & \frac{d^2H_1}{dx^2}\frac{d^2H_4}{dx^2} \\ \frac{d^2H_2}{dx^2}\frac{d^2H_1}{dx^2} & \frac{d^2H_2}{dx^2}\frac{d^2H_2}{dx^2} & \frac{d^2H_2}{dx^2}\frac{d^2H_3}{dx^2} & \frac{d^2H_2}{dx^2}\frac{d^2H_4}{dx^2} \\ \frac{d^2H_3}{dx^2}\frac{d^2H_1}{dx^2} & \frac{d^2H_3}{dx^2}\frac{d^2H_2}{dx^2} & \frac{d^2H_3}{dx^2}\frac{d^2H_3}{dx^2} & \frac{d^2H_3}{dx^2}\frac{d^2H_4}{dx^2} \\ \frac{d^2H_4}{dx^2}\frac{d^2H_1}{dx^2} & \frac{d^2H_4}{dx^2}\frac{d^2H_2}{dx^2} & \frac{d^2H_4}{dx^2}\frac{d^2H_3}{dx^2} & \frac{d^2H_4}{dx^2}\frac{d^2H_4}{dx^2} \end{bmatrix} dx$$

$$[\boldsymbol{K_e}] = \frac{EI}{L^3}\begin{bmatrix} 12 & 6L & -12 & 6L \\ 6L & 4L^2 & -6L & 2L^2 \\ -12 & -6L & 12 & -6L \\ 6L & 2L^2 & -6L & 4L^2 \end{bmatrix} \tag{3.69}$$

3.7. Conventional bar element [Reddy, 1989]

The governing differential equation that is solved using the conventional finite element method, is shown below:

$$EA\frac{d^2u(x)}{dx^2} = 0 \tag{3.70}$$

From the above differential equation, the solution can be obtained as a linear function:

$$u = bx + a \tag{3.71}$$

To determine a and b uniquely for a bar element, the boundary conditions are introduced. Two boundary conditions are needed (displacement related and force related) which can be written as:

$$u(0) = u_1 \; and \; u(L) = u_2 \tag{3.72}$$

$$\begin{bmatrix} u_1 \\ u_2 \end{bmatrix} = \begin{bmatrix} 0 & 1 \\ L & 1 \end{bmatrix} \begin{bmatrix} b \\ a \end{bmatrix} \tag{3.73}$$

The displacement interpolation function for an element can be written as:

$$u(x) = [x \quad 1]\begin{bmatrix} 0 & 1 \\ L & 1 \end{bmatrix}^{-1}\begin{bmatrix} u_1 \\ u_2 \end{bmatrix} = [N^{bar}{}_1 \quad N^{bar}{}_2]\begin{bmatrix} u_1 \\ u_2 \end{bmatrix} = [f]\{d_e\} \tag{3.74}$$

where $[N^{bar}]$ is:

$$[\boldsymbol{N}^{bar}] = \left[1 - \frac{x}{L} \quad \frac{x}{L}\right] \tag{3.75}$$

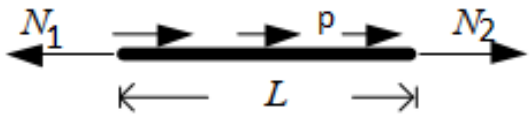

Figure 3.7: Forces applied on a bar element

For a bar element with the length of L shown in Figure 3.7, where N_1 and N_2 are the nodal axial forces and p is the distributed external load, the total potential energy can be written as:

$$\Pi(\mathrm{u}) = \frac{1}{2}\int_0^L EA\left(\frac{du}{dx}\right)^2 dx - \int_0^L pudx + N_1 u\,\big|_{x=0} - N_2 u\,\big|_{x=L} \tag{3.76}$$

By substituting the interpolation function shown in Eq. 3.71 into the first term on the right-hand-side of Eq. 3.76 (strain energy term in the total potential energy), the stiffness matrix of the finite element can be developed as:

$$\begin{aligned} U &= \frac{1}{2}\int_0^L EA\left(\frac{du}{dx}\right)dx = \frac{1}{2}EA\{\boldsymbol{d}_e\}^T\int_0^L\left[\frac{d\boldsymbol{N}^{bar}}{dx}\right]^T\left[\frac{d\boldsymbol{N}^{bar}}{dx}\right]dx\,\{\boldsymbol{d}_e\} \\ &= \frac{1}{2}\{d_e\}^T[K_e]\{d_e\} \Rightarrow\ \delta U = \{\delta d_e\}^T[K_e]\{d_e\} \end{aligned} \tag{3.77}$$

$$[\boldsymbol{K}_e] = EA\int_0^L\left[\frac{d\boldsymbol{N}^{\boldsymbol{bar}}}{dx}\right]^T\left[\frac{d\boldsymbol{N}^{bar}}{dx}\right]dx = EA\int_0^L\begin{bmatrix}-\frac{1}{L}\\ \frac{1}{L}\end{bmatrix}\begin{bmatrix}-\frac{1}{L} & \frac{1}{L}\end{bmatrix}dx \tag{3.78}$$

$$[\boldsymbol{K}_e] = \int_0^L\begin{bmatrix}\frac{EA}{L^2} & -\frac{EA}{L^2}\\ -\frac{EA}{L^2} & \frac{EA}{L^2}\end{bmatrix}dx = \frac{EA}{L}\begin{bmatrix}1 & -1\\ -1 & 1\end{bmatrix} \tag{3.79}$$

3.8. Steady-state analysis using spectral element

The assemblage procedure of the element stiffness matrices is identical to that of the standard displacement-based FEM. As a result of the assemblage the structural dynamic equilibrium can be obtained as

$$[\mathbf{K}(\omega)]\hat{d} = \hat{f} \tag{3.80}$$

in which $[\mathbf{K}(\omega)]$ is the dynamic structural stiffness matrix, $\hat{d}$ is the nodal displacement vector component in the frequency domain and $\hat{f}$ is the Fourier Transform of the excitation. After the displacement field is obtained for each frequency content, the time behavior can be re-constructed as the synthesis of the frequency dependent solutions, i.e., $d(x,t) = \hat{d}(x)e^{i\omega t}$. As a general solution would span the whole frequency range, i.e., $-\infty < \omega < \infty$, the solution in time-domain is obtained from the IFT, i.e.:

$$d(t) = \sum_{n=-\infty}^{\infty} \hat{d}_n e^{in\omega t} \tag{3.81}$$

The essentials of the spectral element solution scheme are the following steps

1. Replacing the input by its spectral form obtained from the Fourier Transform to determine the frequency content.
2. Solving the problem in the frequency domain to obtain the output also in the frequency domain.
3. Reconstruct the response in the time domain by application of the inverse Fourier Transform.

This procedure is show in the Figure 3.8. Figure 3.9 shows the application of the mentioned procedure on a sinusoidal input.

Note that because of the discrete nature of the Fourier transform, the result of the inverse FFT is only valid up to the Nyquist frequency. As suggested in (Doyle 1997), the inverse transform is evaluated only up to the Nyquist, half the sampling frequency, and the remainder is considered as the complex conjugate of the initial part. This ensures that the reconstructed history is real in time domain.

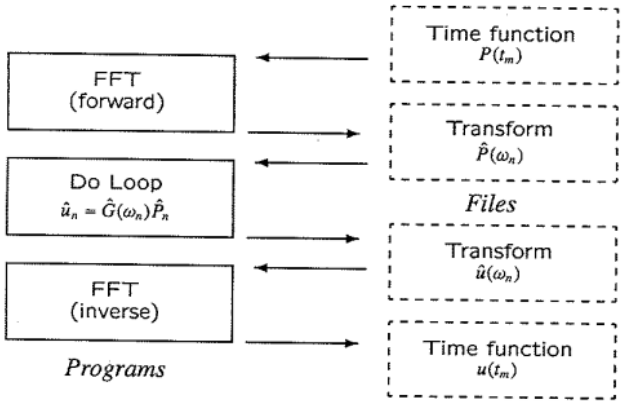

Figure 3.8: Frequency domain analysis and the inverse [Doyle, 1997]

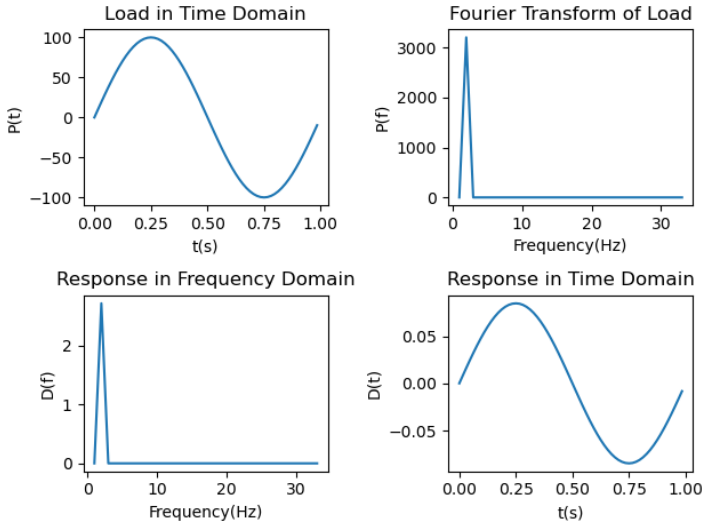

Figure 3.9: Application of the procedure shown in Figure 3.8 on a beam under a sine load

3.9. A discussion on the output of Spectral Finite Element model

To demonstrate the performance of the mentioned method a simple case study is done. A uniform simply supported beam shown in Figure 3.10 made of aluminum with elastic modulus of 10^6 psi and a density of $1.0038 \times 10^{-1} \frac{\text{lb}}{in^3}$ is considered. The length of the beam is $60\ in$. The cross-section of the beam is a rectangle with the height of 4 in and width of 1 in.

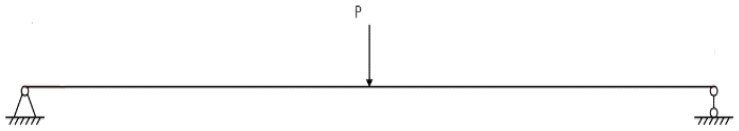

Figure 3.10: Simply supported beam under study

In the first case, the beam is under a concentrated transverse step load in the middle for 1 second with the amplitude of 1000 lbf. In the second test, the beam is under a concentrated sine load with the amplitude of 100 lbf and the frequency of the load changes from 1 Hz to 6 Hz. Fig 3.11 shows the applied step load and the sine load with the frequency of 1 Hz.

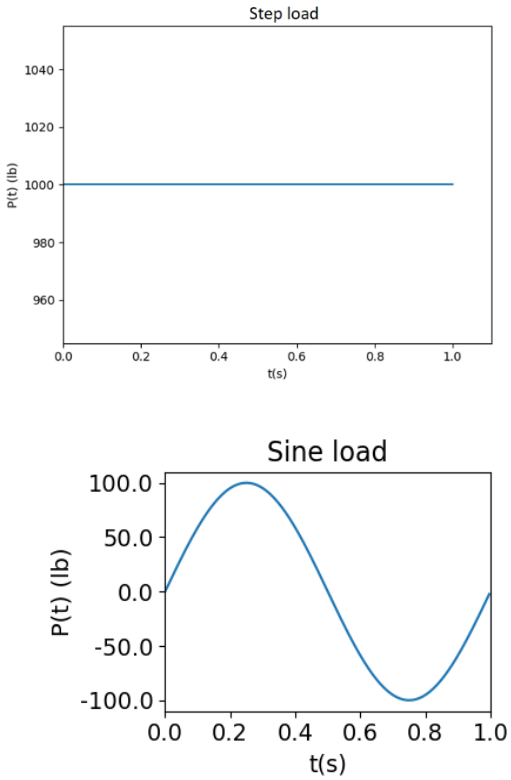

Figure 3.11: Step and sine load functions

The beam is modelled using two spectral beam elements and the lateral displacement of the middle point of the beam is captured using spectral elements and compared with the results from analytical solutions in Figure 3.12.

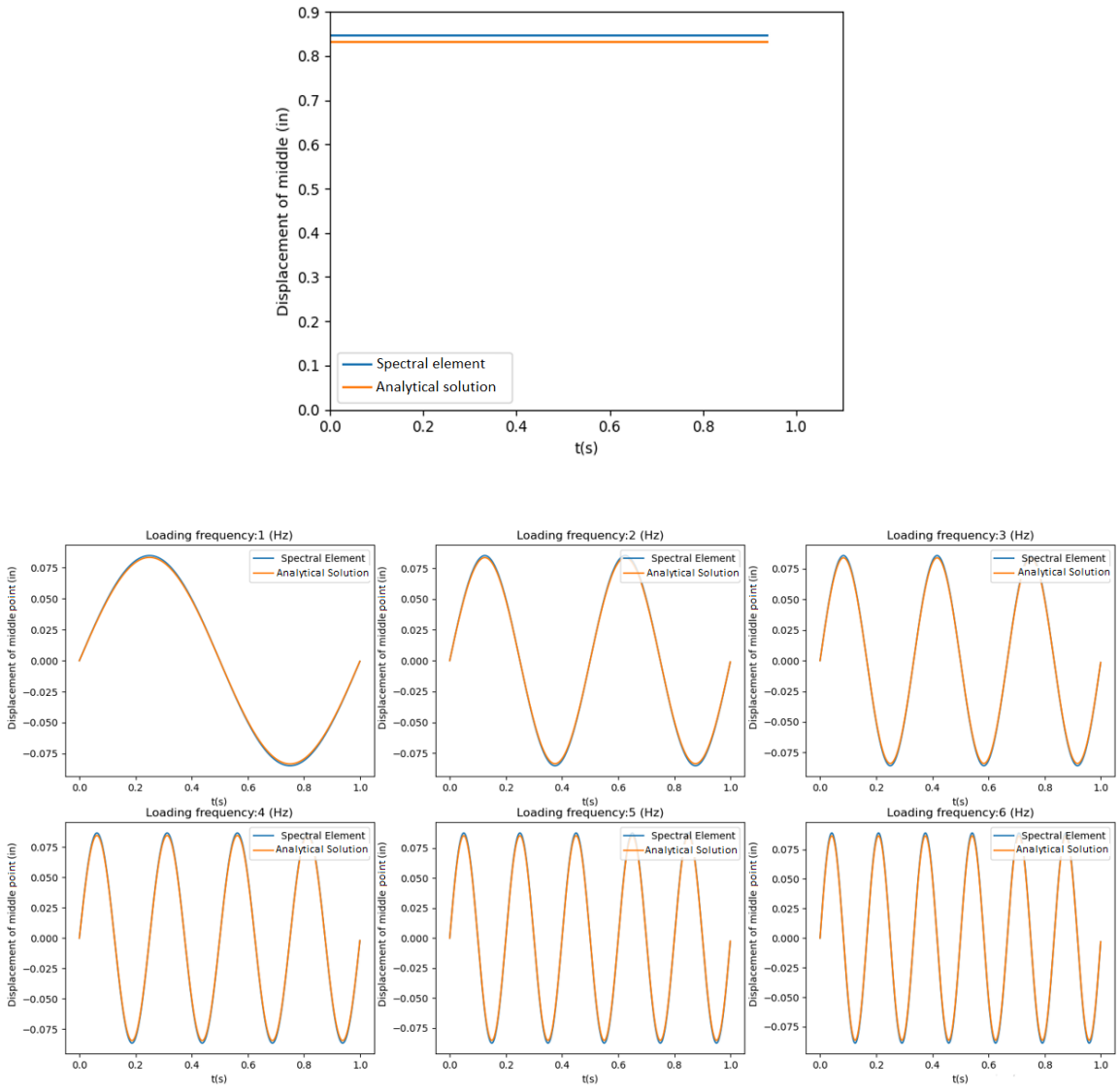

Figure 3.12: Steady-state transverse displacement of the middle point of the beam under step and sine loads

3.10. The missing part (transient part)

As shows in Figure 3.12, the response gained from Fourier analysis is in the frequency of the excitation only, however it is expected to see other terms that are in the frequency of the structure

in an undamped vibration response. Consider the equation of motion of an undamped single-degree-of-freedom system under a harmonic load as:

$$m\ddot{x} + kx = p\ sin\omega t \tag{3.82}$$

With the initial conditions below:

$$x = x(0), \dot{x} = \dot{x}(0) \tag{3.83}$$

The particular solution to Eq. 3.82 is :

$$x_p(t) = \frac{p}{k}\frac{1}{1-\left(\frac{\bar{\omega}}{\omega_n}\right)^2} sin\bar{\omega}t \tag{3.84}$$

The complementary solution is the free vibration response:

$$\mathrm{x}_c(\mathrm{t}) \ = \ \mathrm{A}\ \mathrm{sin}\omega_n\mathrm{t} \ + \ \mathrm{Bcos}\omega_n\mathrm{t} \tag{3.85}$$

The total response will be:

$$x(t) = \mathrm{A}\ \mathrm{sin}\omega_n\mathrm{t} \ + \ \mathrm{Bcos}\omega_n\mathrm{t} + \frac{p}{k}\frac{1}{1-\left(\frac{\bar{\omega}}{\omega_n}\right)^2} sin\bar{\omega}t \tag{3.86}$$

By imposing the initial conditions, the constants A and B are determined, and the equation above is rewritten as:

$$x(t) = x(0)cos\omega_n t + \left[\frac{\dot{x}(0)}{\omega_n} - \frac{p}{k}\frac{\frac{\bar{\omega}}{\omega_n}}{1-\left(\frac{\bar{\omega}}{\omega_n}\right)^2}\right]\sin\omega_n t + \frac{p}{k}\frac{1}{1-\left(\frac{\bar{\omega}}{\omega_n}\right)^2} sin\bar{\omega}t \tag{3.87}$$

The response can also be written using Duhamel's integral as:

$$x(t) = x(0)cos\omega_n t + \frac{\dot{x}(0)}{\omega_n}\sin\omega_n t + \int_0^t h(\tau)\sin\bar{\omega}(\mathrm{t}-\tau)d\tau \tag{3.88}$$

where:

$$h(\tau) = \frac{1}{m\omega_n} p(\tau) \tag{3.89}$$

Comparing Eq. 3.88 and Eq. 3.87, the equation below is written:

$$\int_0^t h(\tau)\sin\bar{\omega}(\mathrm{t}-\tau)d\tau \;=\; \frac{p}{k}\frac{\frac{\bar{\omega}}{\omega}}{1-\left(\frac{\bar{\omega}}{\omega_n}\right)^2}\sin\omega_n t + \frac{p}{k}\frac{1}{1-\left(\frac{\bar{\omega}}{\omega_n}\right)^2}sin\bar{\omega}t \tag{3.90}$$

The left-hand side of Eq. 3.90 can be rewritten as:

$$\int_0^t h(\tau)\sin\bar{\omega}(\mathrm{t}-\tau)d\tau \;=\; \int_0^\infty h(\tau)\sin\bar{\omega}(\mathrm{t}-\tau)d\tau \;-\; \int_t^\infty h(\tau)\sin\bar{\omega}(\mathrm{t}-\tau)d\tau \tag{3.91}$$

The term $\int_0^\infty h(\tau)\sin\bar{\omega}(\mathrm{t}-\tau)d\tau$ on the right-hand side of Eq. 3.91 can be expressed in the frequency domain using Fourier transform. It is the part of the response that is determined in spectral analysis and is in the frequency of the excitation. This term is equivalent to the first term on the right-hand side of Eq. 3.87, i.e. $\frac{p}{k}\frac{1}{1-\left(\frac{\bar{\omega}}{\omega_n}\right)^2}sin\bar{\omega}t$ .Consequently, the term $-\int_t^\infty h(\tau)\sin\bar{\omega}(\mathrm{t}-\tau)d\tau$ in Eq. 3.91 is equivalent to $x(0)cos\omega_n t + \left[\frac{\dot{x}(0)}{\omega_n} - \frac{p}{k}\frac{\frac{\bar{\omega}}{\omega_n}}{1-\left(\frac{\bar{\omega}}{\omega_n}\right)^2}\right]sin\omega_n t$ in Eq. 3.87. While the Fourier Transform brings in the particular solution, the transient response must be added to have the complete response.

A summary of the Spectral Element solution procedure is shown in Figure 3.13. In Spectral Element Analysis, it is essential to replace the external excitation by its spectral form using the Fourier Transform to determine its frequency content. By doing this the problem can be solved in the frequency domain to obtain the output also in the frequency domain. The reconstructions in the time domain are then done by application of the inverse Fourier Transform and this completes the Steady-State solution. As it will be discussed in the following sections, the response obtained from the Inverse Fourier Transform is incomplete and does not contain the free vibration component. To obtain the Transient response, the natural frequencies of the system need to be identified.

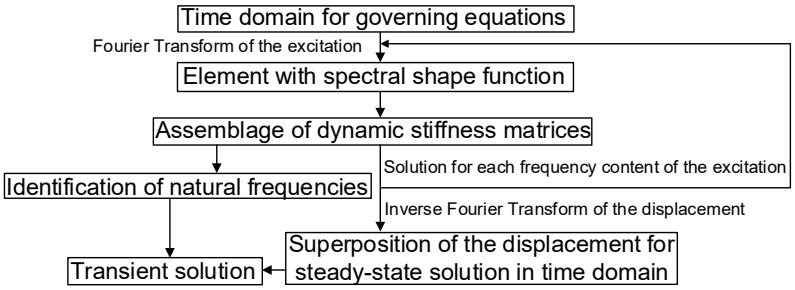

Figure 3.13: Complete spectral analysis procedure

3.11. Addition of the transient response

[Veletsos and Kumar, 1983] developed a procedure based on the solution of the dynamic differential equation, in which the steady-state solution can be used to identify the additional transient contribution for systems that are starting from at rest state. This method can simply be extended to multi-degree-of-freedom systems using modal analysis as each mode can be treated to constitute a single-degree-of-freedom system. Herein, the method by [Veletsos and Kumar, 1983] has been adopted on an ad-hoc basis by using the shape functions obtained from the spectral method within the mode shapes.

In a single-degree-of-freedom system the general solution of the below differential equation subject to the given initial conditions

$$m\ddot{x} + kx = p\ sin\bar{\omega}t\ ,\ x(0) = 0\ ,\ \dot{x}(0) = 0 \tag{3.92}$$

consists of the particular solution, that is:

$$x_p(t) = \frac{p}{k}\frac{1}{1-\left(\frac{\bar{\omega}}{\omega_n}\right)^2} sin\bar{\omega}t \tag{3.93}$$

and the complementary solution, which is the free vibration response:

$$\mathrm{x}_c(\mathrm{t}) = \mathrm{A}\ \mathrm{sin}\omega_n\mathrm{t} + \mathrm{B}\ \mathrm{cos}\omega_n\mathrm{t} \tag{3.94}$$

where ω_n is the natural frequency of the system.

By imposing the initial conditions, the constants A and B are determined, and the total solution can be obtained as:

$$x(t) = \frac{p}{k}\frac{1}{1-\left(\frac{\bar{\omega}}{\omega_n}\right)^2} sin\bar{\omega}t + \frac{p}{k}\frac{\frac{\bar{\omega}}{\omega}}{1-\left(\frac{\bar{\omega}}{\omega_n}\right)^2} sin\,\omega_n t \tag{3.95}$$

If the result from spectral analysis is shown with $y(t)$ and the total response is shown with $x(t)$, the difference between these two can be written as a corrective function ϵ(t) as [Veletsos, Kumar, 1983]:

$$\epsilon(t) = x(t) - y(t) \tag{3.96}$$

ϵ(t) represents the effect of unsatisfied initial conditions. Consequently, one can write:

$$\epsilon(\mathrm{t}) = \epsilon\,(0)cos\omega t + \frac{\dot{\epsilon}\,(0)}{\omega}\sin\omega t \tag{3.97}$$

Using Eq. 3.96, one can write for the system introduced in Eq. 3.92:

$$\epsilon(0) = \mathrm{x}(0) - \mathrm{y}(0) = 0\ ,\ \dot{\epsilon}(0) = \dot{\mathrm{x}}(0) - \dot{\mathrm{y}}(0) = -\frac{p\bar{\omega}}{k}\frac{1}{1-\left(\frac{\bar{\omega}}{\omega_n}\right)^2} \tag{3.98}$$

For multi-degree-of-freedom systems, the steady-state response, i.e. y(t), can be expressed in terms of modes of vibration as:

$$\{y(t)\} = \sum_{i=1}^{n}\{\boldsymbol{\phi}_i\}\, r_i(t) \tag{3.99}$$

where $\{\boldsymbol{\phi}_i\}$ is the vector of ith mode of displacement and $r_i(t)$ is the modal coordinate.

Also, one can write:

$$\{x(t)\} = \sum_{i=1}^{n}\{\boldsymbol{\phi}_i\}\,[r_i(t) + \alpha_i(t)] \tag{3.100}$$

where $\alpha_i(t)$ is the modal coordinate for the transient part. Considering that structure is initially at rest, i.e.

$$\{\dot{\epsilon}(t)\} = \sum_{i=1}^{n} \{\boldsymbol{\phi}_i\} \frac{\dot{\alpha}_\iota(0)}{\omega} \sin \omega t\ (t) \tag{3.101}$$

Hence one can calculate $\dot{\alpha}_\iota(0)$ as:

$$\dot{\alpha}_\iota(0) = \frac{\{\boldsymbol{\phi}_i\}^T [M](\{\dot{\boldsymbol{x}}(0)\} - \{\dot{\boldsymbol{y}}(0)\})}{\{\boldsymbol{\phi}_i\}^T [M]\{\boldsymbol{\phi}_i\}} \tag{3.102}$$

Note that the mode shapes and frequencies are calculated from the dynamic stiffness matrix and $[\boldsymbol{M}]$ is the lumped mass matrix, which introduces some spatial discretization error to the transient solution.

3.12. Calculation of natural frequencies [Wittrick and Williams, 1970]

The problem of determining natural frequencies of vibration of a finite element model is solved by determining the eigenvalues of the linear eigenvalue problem shown in Eq. 3.103:

$$([\boldsymbol{K}] - \omega^2[\boldsymbol{M}])\ \{\boldsymbol{D}\} = 0 \tag{3.103}$$

where [**K**] is the finite element stiffness matrix and [**M**] is the mass matrix.

For the spectral element method, since the exact dynamic shape functions are used, the dynamic stiffness matrix is a transcendental function of ω. The natural frequencies are determined by finding the eigenvalues of the transcendental equation in Eq. 3.104.

$$([\boldsymbol{K}(\omega)]\ )\ \{\boldsymbol{D}\} = 0 \tag{3.104}$$

The effect of distributed mass is considered in $\boldsymbol{K}(\omega)$.

[Wittrick and Williams,1970] proposed a method to find the eigenvalues of a transcendental problem. The method is based on counting the number of eigenvalues exceeded by a certain value, ω^*. The main idea of the method relies on the following statement:

"If a structure whose natural frequencies, written in ascending order, ω_r (r=1,2, 3…) has one constraint imposed upon it, the natural frequencies of the constrained structure, shown by ω_r', satisfy: $\omega_r \leq \omega_r' \leq \omega_{r+1}$" [Wittrick and Williams, 1970]

It can be understood from the statement above that if n constraints are applied to a structure and removed one by one, as each constraint is removed the number of natural frequencies exceeded by ω^*will stay the same or increase by one. So, the number of natural frequencies less than ω^* can be calculated with the given formula in [Wittrick and Williams, 1970]:

$$J(\omega^*) = J_0(\omega^*) + s[\boldsymbol{K}(\omega^*)] \tag{3.105}$$

$s[\boldsymbol{K}(\omega^*)]$ is the sign count of the $\boldsymbol{K}(\omega^*)$ and is equal to the number of negative values on the diagonal of the upper triangular matrix $\boldsymbol{K}(\omega^*)$. The procedure employs the upper triangular matrix $\mathbf{K_\Delta}(\omega)$ that is obtained from $\boldsymbol{K}(\omega)$ using the usual form of Gauss elimination, in which rows are taken as pivotal in order, and appropriate multiples of the pivotal row are added to succeeding rows, making all elements below the pivot zero.

As explained in [Wittrick and Williams, 1970], the idea of the method is that since the determinant of $\boldsymbol{K}(\omega^*)$ is equal to multiplying all the values on the diagonal of the upper triangular $\mathbf{K_\Delta}(\omega^*)$, any negative value on the diagonal represents exceeding a root of $|\boldsymbol{K}(\omega^*)| = 0$ for $\omega < \omega^*$.

Assume a structure with constraints on its all degrees of freedom, if f and f+1 constraints are released, the following relationship can be written as Eq. 3.106 and shown in Figure 3.14.

$$\left|\boldsymbol{K}_{f+1}\right| = \left|\boldsymbol{K}_f\right| * \boldsymbol{K}^{\Delta}_{f+1,f+1} \tag{3.106}$$

If $K^{\Delta}_{f+1,f+1}$ is negative, a change in the sign of $|\mathbf{K}|$ is happened. If all the constraints are released, $s[\boldsymbol{K}(\omega^*)]$ shows the number of natural frequencies less than ω^*.

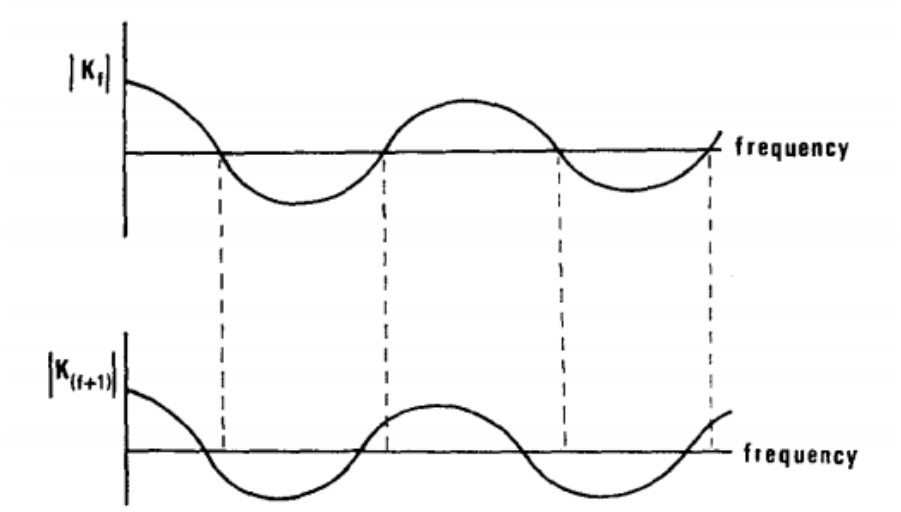

Figure 3.14: Effect of releasing a constraint on the determinant of the dynamic stiffness matrix [Wittrick and Williams, 1970]

3.13. Calculation of J0

J_0 is the value which J would have had if constraints had been imposed on the structure to nullify all the displacements $\boldsymbol{d}$, so that $\boldsymbol{d} = 0$. Therefore, when $\boldsymbol{d} = 0$ the structure degenerates into its component members in isolation, with their ends clamped, i.e. $J_0 = \sum J_m$ in which summation extends over all the members and J_m is the number of natural frequencies lying between zero and the trial value of $\bar{\lambda}$, for a member with its ends clamped.

According to [Wittrick and Williams, 1970], natural frequencies of a member with its ends clamped will occur when one or more elements on the dynamic stiffness matrix of the system are infinite. The following formulas are given in [Wittrick and Williams, 1970] by setting the terms on the dynamic stiffness matrix of a frame element to zero.

$$J_m = J_a + J_b \tag{3.107}$$

where:

$$J_a \text{ is the highest integer} < \frac{\omega l}{\pi}\sqrt{\frac{\mu}{EA}} \tag{3.108}$$

and:

$$J_b = i - \frac{1}{2}\left[1 - (-1)^i sg(1 - cosh\lambda\, cos\lambda)\right], \lambda = \sqrt[4]{\frac{\omega^2 \mu l^4}{EI}} \tag{3.109}$$

where i is the highest integer $< \frac{\lambda}{\pi}$ and $sg(1 - cosh\lambda\, cos\lambda)$ is +1 or -1 depending upon the sign of $(1 - cosh\lambda\, cos\lambda)$.

3.14. Bisection method [Epperson, 2013]

Bisection method is a simple iterative technique for determining roots of a function. The basis of the method can be illustrated for a generic nonlinear function which is plotted in Figure 3.15:

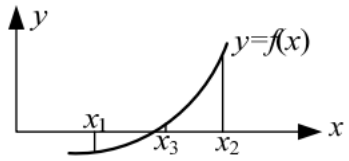

Figure 3.15: Trial points in Bisection method

We can begin finding the root of the function by picking two values x_1 and x_2 such that $f(x_1)f(x_2) < 0$. That means when one of the functional values is negative the other is positive and for a continuous function the root must lie between x_1 and x_2 . A new approximation to the root can be calculated as:

$$x_3 = \frac{x_1 + x_2}{2} \tag{3.110}$$

As illustrated in the figure above in the case of $f(x_1)f(x_3) < 0$, x_1 and x_2 can be used to compute another value. Otherwise, x_2 and x_3 is used. The process is continued until the desired accuracy is achieved, i.e. f (x) ≈ 0.

The same idea can be used to look for the i^{th} natural frequency. We begin by taking values ω_1 and ω_2 such that $J(\omega_1) < J(\omega_2)$. This means that there must be at least one natural frequency between ω_1 and ω_2. A new approximation of the natural frequency is calculated as:

$$\omega_3 = \frac{\omega_1 + \omega_2}{2} \tag{3.111}$$

if $J(\omega_1) < J(\omega_3)$, ω_1 and ω_3 are used to calculate a new value. Otherwise, ω_2 and ω_3 are used. This process is repeated until the difference in ω for two consecutive trials becomes less than the desired precision. After the first natural frequency is found this process is repeated by taking the lower bound as the natural frequency found in the previous step and repeating.

3.15. Calculation of mode shapes

Substituting each natural frequency into the dynamic stiffness matrix and solving $[\boldsymbol{K}(\omega)]\{\boldsymbol{d}\} = 0$ for $\{\boldsymbol{d}\}$, gives the modes of vibration. The rows or the columns of the $\mathbf{K}(\omega)$ are linearly dependent. So, the eigenvector is determined by assuming an arbitrary value for one of the terms on $\{\mathbf{d}\}$ and solving for the rest.

3.16. Damage detection

Spectral Finite Element provides a computationally efficient tool to calculate as many vibration modes and frequencies as desired. The efficiency is due to the fact that there is no need for mesh refinement to get access to higher modes. Structural damage usually causes stiffness reduction, which is reflected as a decrease in natural frequencies and change in vibration mode shapes. Furthermore, measuring natural frequencies and mode shapes is easily applicable through sensor measurements since they are global characteristics of the structure.

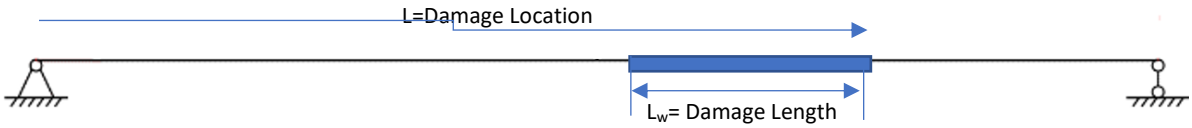

Figure 3.16: Damage Model

Consider the simply supported beam in Figure 3.16, with a cracked element inside. The properties of the cracked element can be addressed using the following parameters:

L: Location of the damaged element

L_w : Length of the damaged element

D: Damage index

D is the reduction ratio in E due to cracks and has a value between 0 and 1. Elasticity modulus of the cracked element is related to the elasticity modulus of the healthy element with Eq. 3.112:

$$E_{Cracked} = (1 - D)E \tag{3.112}$$

3.17. Effect of damage on natural frequencies

To illustrate the effect of damage on vibration characteristics of a beam, consider the structure in Figure 3.16. The beam is 60 in long and a damaged element with the constant length of 5 in is moved across the length of the beam. The damage index varies from 0.1 to 0.9 with a 0.1 step. The relative difference due to damage in the first three natural frequencies are shown in Figures 3.17, 3.18, 3.19.

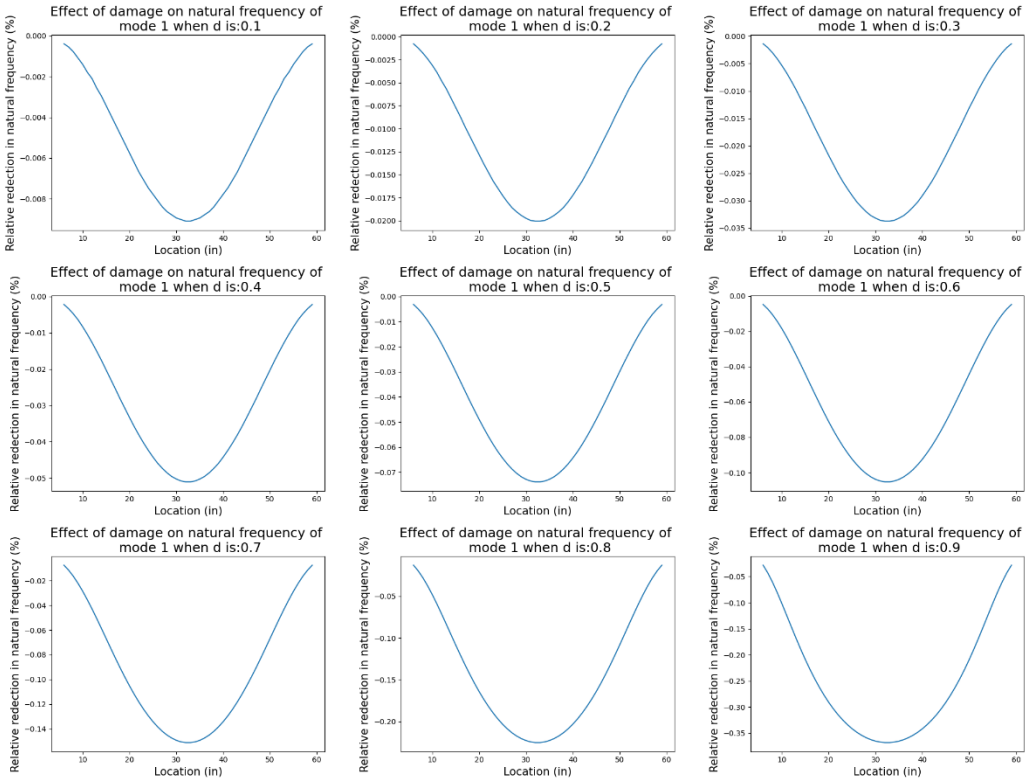

Figure 3.17: Effect of moving the damaged element along the length of the beam on the first frequency of vibration

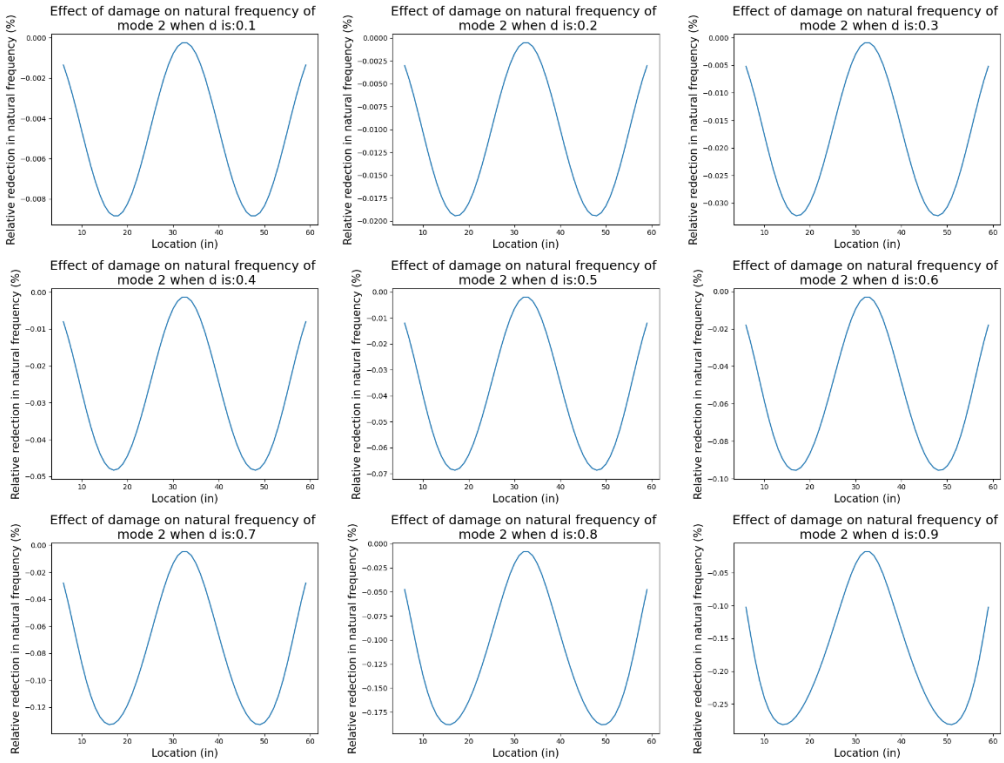

Figure 3.18: Effect of moving the damaged element along the length of the beam on the second frequency of vibration

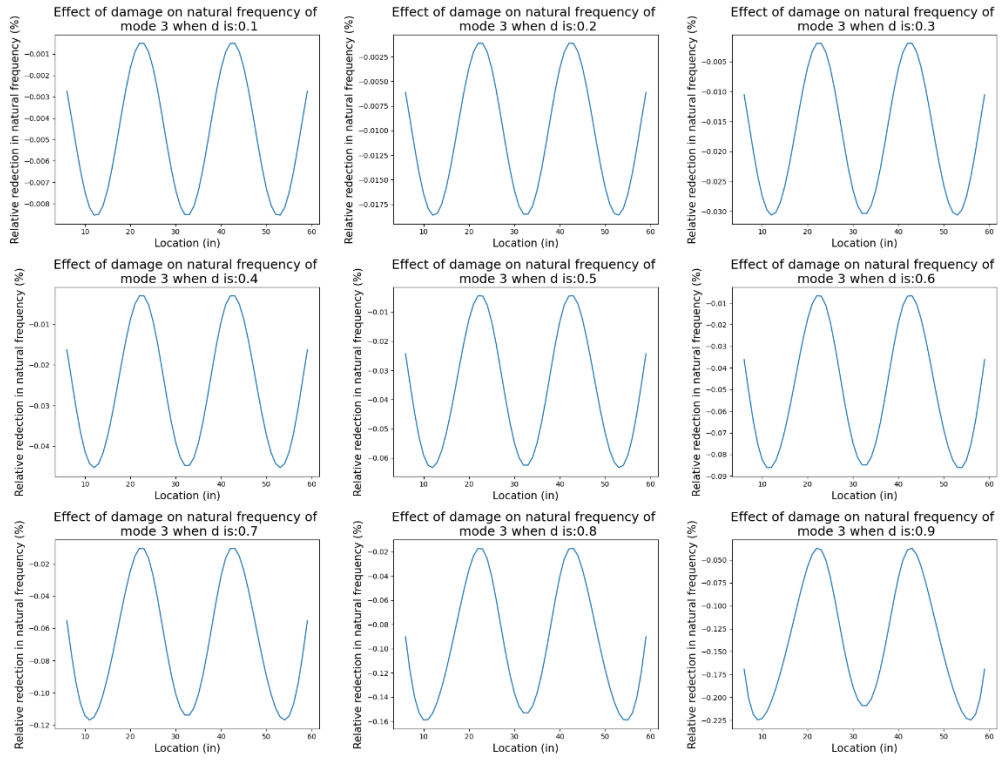

Figure 3.19: Effect of moving the damaged element along the length of the beam on the third frequency of vibration

Figure 3.17 shows the first natural frequency affected by damage the most when it is located in the middle. On the contrary, the frequency of the second mode changes the least when damage is in the middle. For the first mode, this happens when damage is at the beginning or end. This illustrates the importance of considering higher modes since some damage cases might not change the frequency of one mode as noticeably as another.

3.18. Damage cost function:

Assume that the first n natural frequencies and corresponding mode shapes of a cracked structure are measured as ($\lambda^{exp}, \phi^{exp}$). The purpose of the damage detection tool is to put a damaged element inside the healthy structure in a way that the location, the length, and the damage index match the real structure. So, a trial damaged model is created, and the first n natural frequencies and mode shapes are calculated using spectral element analysis ($\lambda^{trial}, \phi^{trial}$).

As suggested in [Dong and Wang, 2019], the cost function in Eq. 3.113, gives a comparison metric indicating how close the trial structure is to the real structure. The first term gives the relative difference in natural frequencies. The second term takes in two vectors at each step, the i^{th} mode shape from measurement and the i^{th} mode shape from the trial structure. MAC (modal assurance criterion) takes on values from zero- representing no consistent correspondence, to one- representing a consistent correspondence. If the modal vectors exhibit a consistent linear relationship, the modal assurance criterion should approach unity. Note that the MAC value is normalized by magnitude of input vectors and is bounded by zero and one [Allemang, 2003].

$$Cost(\{\lambda\}^{trial}, \{\Phi\}^{trial}, \{\lambda\}^{exp}, \{\Phi\}^{exp}) \tag{3.113}$$

$$= \sum_{i=1}^{n} \left(\frac{\lambda_i^{exp} - \lambda_i^{trial}}{\lambda_i^{exp}} . w_{\lambda_i} \right)^2 + \left(\frac{1 - \sqrt{MAC_i(\{\phi_i^{exp}\}, \{\phi_i^{trial}\})}}{\sqrt{MAC_i(\{\phi_i^{exp}\}, \{\phi_i^{trial}\})}} . w_{\phi_i} \right)^2$$

$\{\lambda\}^{exp} = \{ \lambda_1^{exp}, \lambda_2^{exp}, \dots, \lambda_n^{exp} \}$, $\{\lambda\}^{trial} = \{ \lambda_1^{trial}, \lambda_2^{trial}, \dots, \lambda_n^{trial} \}$

$$MAC_i\left(\{\phi_i^{exp}\},\{\phi_i^{trial}\}\right)=\frac{\left(\{\phi_i^{exp}\}^T.\{\phi_i^{trial}\}\right)^2}{\left(\{\phi_i^{exp}\}^T.\{\phi_i^{exp}\}\right)\left(\{\phi_i^{trial}\}^T.\{\phi_i^{trial}\}\right)} \tag{3.114}$$

The weights w_{λ_i} and w_{ϕ_i} are set to 1 in this study, meaning that all modes have an equal contribution to the cost function. This provides the opportunity to investigate the effect of considering more number of modes on the performance of the damage detection program as done in Chapter 4.

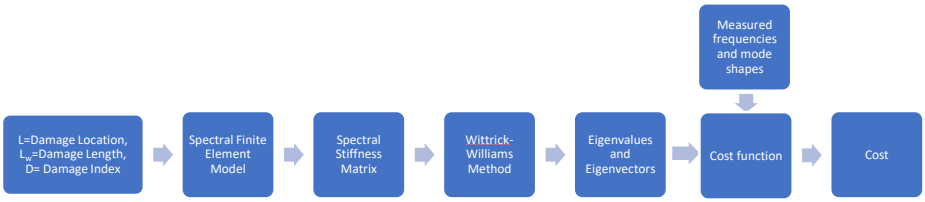

Figure 3.20: Calculation of the cost of each trial structure

The diagram in Figure 3.20 shows how for each set of $\{L^{trial}, L_w^{trial}, D^{trial}\}$, a cost value is found. The problem is minimizing the cost function by changing $\{L^{trial}, L_w^{trial}, D^{trial}\}$ within the given constraints given in Eq 3.115:

$$minimize\left[Cost\left(\{\lambda\}^{trial},\{\Phi\}^{trial}\right)\right] \tag{3.115}$$

Subject to:

$$0 < L_w^{trial} < L_w^{max}$$

$$0 < L^{trial} < L_{beam}$$

$$0 < D < 1.0$$

To visualize the behavior of the cost function for different trial models, a damaged structure with these specifics $\{L^{trial} = 50\ in, L_w^{trial} = 8\ in, D^{trial} = 0.3\}$ is modelled and the cost function is calculated for different trial structures compared to the original damaged structure by moving a damaged element with a variable length along the length of the beam. Figure 3.21 shows that the cost function is a complicated function of the damaged element specifics and a robust optimization

technique independent of the nature of the function should be adopted to minimize the cost to find the closest model.

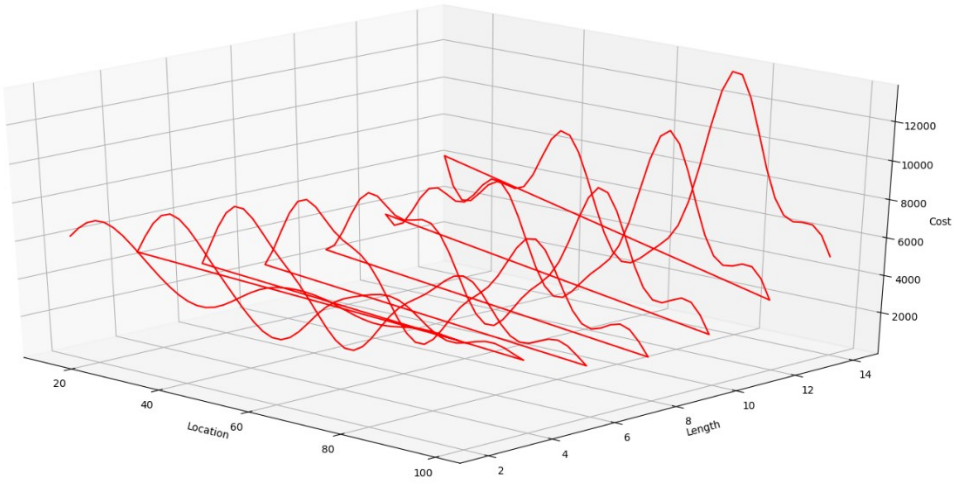

Figure 3.21: Cost of each trial as a function of length and location of the damaged element showing the optimization space

3.19. Genetic algorithm

Genetic algorithms are search algorithms based on the mechanics of natural selection and natural genetics. They combine survival of the fittest string with a structured yet randomized information exchange to form a search algorithm. In every generation a new set of artificial strings is created using bits and pieces of the fittest of the old. While randomized, genetic algorithms are no simple random walk. They efficiently exploit historical information to speculate on new search points with expected improved performance.

Genetic algorithms have been developed by John Holland, his colleagues and his students at the University of Michigan. The goal of their research was, 1) to abstract and explain the adaptive processes of natural systems and 2) to design artificial systems that retain the important mechanisms of natural systems.

Calculus-based optimization methods are subdivided into two main classes [Goldberg, 1988]:

1) Indirect methods seek local extrema by solving the usually nonlinear set of equations resulting from setting the gradient of the objective function equal to zero. Given a smooth unconstrained function, finding a possible peak starts by restricting search to those points with slopes of zero in all directions.
2) Direct methods seek local optimal by hopping on the function and moving in direction related to the local gradient. This is simply the notion of hill climbing: to find the local best climb the function in the steepest permissible direction.

Calculus-based methods show lack of robustness for two reasons. Firstly, both methods are local in scope. The optima they seek is the best in the neighborhood of the starting point. Secondly, calculus-based methods depend on existence of their derivatives even if we allow a numerical approximation of their derivatives, this is a severe shortcoming

[Hong, Yong 2002] GAs are based on principles of evolutionary theory such as natural selection and evolution. Each possible solution is called a chromosome and consists of multiple genomes. A possible solution is shown in Figure 3.22.

Damage Location	Damage Length	Damage Index
0 1 0 0 0 0 0	1 0 1 0 0	0 0 1 0 1 1 1

Figure 3.22: A possible solution shown in binary

Fitness function indicates how close the candidate solution is to the real solution. The cost function in Eq 3.114 is taken as the fitness in this study. Obviously, since we are solving a minimization problem, the lower the fitness value, the better solution the corresponding chromosome is. A generation includes a set of chromosomes. The population size can differ depending on the problem. Reproduction is the process of creating a new generation based on the previous generation. Reproduction is done through crossover and mutation. In this study the generation size was taken as 8. The first generation is produced randomly within the constraints in Eq 3.115. The population is sorted based on the fitness of candidates in it. The two best candidates in the first generation are moved directly to the next generation. The rest of the next population is generated through pair selection, crossover, and mutation. First generation is generated randomly between the constraints of the problem and an example of such generation is shown in Figure 3.23:

Candidate Number	Damage Location	Damage Length	Damage Index
1	0 1 0 0 0 0 0	1 0 1 0 0	0 0 1 0 1 1 1
2	0 1 0 1 0 0 1	1 0 1 1 0	1 0 1 0 1 1 1
3	0 0 1 1 0 0 0	0 0 0 1 1	0 0 1 1 1 1 1
4	0 1 0 0 0 1 0	0 1 0 0 0	0 0 0 1 1 0 0
5	0 1 1 0 0 0 0	0 0 1 0 0	1 0 0 0 0 1 0
6	0 1 0 1 1 0 0	1 0 0 0 0	1 0 1 1 0 0 0
7	0 0 1 0 0 1 0	0 0 1 1 1	0 0 0 1 1 1 1
8	0 0 0 1 1 1 1	1 0 0 0 0	0 1 0 1 1 0 0

Figure 3.23: First generation of candidate solutions generated randomly within the constraints of the problem.

Pair selection:

In a population of size n like $[x_1, x_2, x_3, \dots, x_n]$ with the corresponding fitness values $[f_1, f_2, f_3, \dots, f_n]$, the candidate with a lower fitness value, has a better chance of entering the next generation. So, the possibility of each chromosome entering the reproduction process is shown as $[p_1, p_2, p_3, \dots, p_n]$ and calculated as Eq. 3.116:

$$P_i = 1 - \frac{fitness_i}{\sum_{i=1}^{population\ size} fitness_i}, i = 1,2,3,..,n \quad (3.116)$$

Cross-over:

Assume two chromosomes selected after pair-selection like, $x_i = [x_{i1}, x_{i2}, x_{i3}, \dots, x_{im}]$ and $x_j = [x_{j1}, x_{j2}, x_{j3}, \dots, x_{jm}]$. If the elements after the kth element on x_i are swapped with the ones on x_j, the new chromosomes will be, $x_i = [x_{i1}, x_{i2}, x_{i3}, \dots, x_{ik}, x_{j(k+1)}, \dots, x_{jm}]$ and $x_j = [x_{j1}, x_{j2}, x_{j3}, \dots, x_{jk}, x_{i(k+1)}, \dots, x_{im}]$. In this study multi-point crossover was used. Since each chromosome consists of genes representing $\{L^{trial}, L_w^{trial}, D^{trial}\}$, the cross over is done on three points, each for one parameter. The value of j,t,u in the example below are randomly selected.

$$x_1 = \left\{L_{11}, L_{12}, \dots, L_{1m}, L_{w11}, L_{w12}, \dots, L_{w1p}, D_{11,}D_{12}, \dots, D_{1q}\right\} \quad (3.117)$$

$$x_2 = \left\{L_{21}, L_{22}, \dots, L_{2m}, L_{w11}, L_{w22}, \dots, L_{w2p}, D_{21,}D_{22}, \dots, D_{2q}\right\}$$

$$x'_1 = \{L_{11}, L_{12}, \dots, L_{1j}, L_{2(j+1)}, \dots, L_{2m}, L_{w11}, L_{w12}, \dots, L_{w1t}, L_{w2(t+1)}, \dots, L_{w2p}, D_{11,}D_{12}, \dots, D_{1u}, D_{2(u+1)}, \dots, D_{2q}\}$$

$$x'_2 = \{L_{21}, L_{22}, \dots, L_{2j}, L_{1(j+1)}, \dots, L_{1m}, L_{w21}, L_{w22} \dots, L_{w2t}, L_{w1(t+1)}, \dots, L_{w1p}, D_{21,}D_{22}, \dots, D_{2u}, D_{1(u+1)}, \dots, D_{1q}\}$$

Mutation:

Sometimes the solution gets trapped around a local minimum instead of the global minimum. During mutation one of the genomes is randomly selected and its value is changed from 0 to 1 or from 1 to 0. This brings new solutions to evolution that might have better answers than what is already in the population. The probability of mutation was taken 0.5 in this study. The mutation process is shown in Figure 3.24.

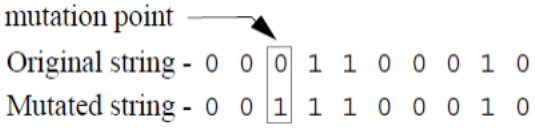

Figure 3.24: Mutation

Parameters such as population size and mutation probability are generally chosen based on trial and error. During the trial-and-error process, it was observed that a small population size made the solutions present in the generation less diverse and that the program could easily get stuck around local minimums. The mutation process was also chosen in a way to help having a more diverse set of candidates in the generation to avoid local minimums.

3.20. Composite Laminate [Lee, 2009]

It is well recognized that fiber reinforced composite materials have many advantages over isotropic materials due to their high strength-to-density ratios. Thus, they have been widely used in many industrial applications. Typical examples are composite aircraft wings, helicopter blades, propeller blades, turbine blades, axles of vehicles and so on. In general, the laminated composite structures are fabricated by bonding two or more laminates together.

Stress-strain relationships on a 3D element

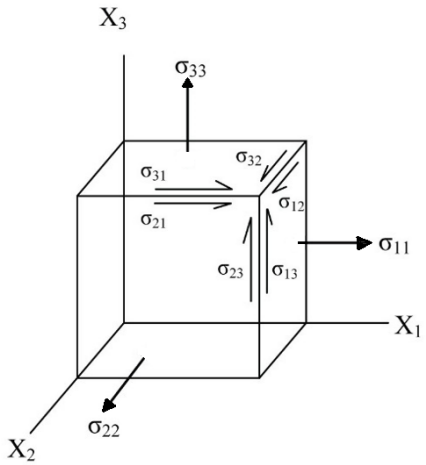

Figure 3.25: Stresses applied on a 3D element

For an orthotropic material, it is known that the strain-stress relationships can be written as:

$$\begin{Bmatrix} \varepsilon_1 \\ \varepsilon_2 \\ \varepsilon_3 \\ \varepsilon_4 \\ \varepsilon_5 \\ \varepsilon_6 \end{Bmatrix} = \begin{bmatrix} S_{11} & S_{12} & S_{13} & 0 & 0 & 0 \\ S_{12} & S_{22} & S_{23} & 0 & 0 & 0 \\ S_{13} & S_{23} & S_{33} & 0 & 0 & 0 \\ 0 & 0 & 0 & S_{44} & 0 & 0 \\ 0 & 0 & 0 & 0 & S_{55} & 0 \\ 0 & 0 & 0 & 0 & 0 & S_{66} \end{bmatrix} \begin{Bmatrix} \sigma_1 \\ \sigma_2 \\ \sigma_3 \\ \sigma_4 \\ \sigma_5 \\ \sigma_6 \end{Bmatrix} \tag{3.118}$$

where σ_i denotes stress and ε_i denotes strain in different directions and S_{ij} are given as:

$$S_{11} = \frac{1}{E_1}, S_{22} = \frac{1}{E_2}, S_{33} = \frac{1}{E_3} \tag{3.119}$$

$$S_{44} = \frac{1}{G_{23}}, S_{55} = \frac{1}{G_{31}}, S_{66} = \frac{1}{G_{12}}$$

$$S_{12} = -\frac{\nu_{21}}{E_2}, S_{13} = -\frac{\nu_{31}}{E_3}, S_{23} = -\frac{\nu_{32}}{E_3}$$

σ_i and ε_i are short-form notations for:

$$\sigma_1 = \sigma_{11}, \sigma_2 = \sigma_{22}, \sigma_3 = \sigma_{33}, \sigma_4 = \sigma_{23}, \sigma_5 = \sigma_{31}, \sigma_6 = \sigma_{12} \tag{3.120}$$

$$\varepsilon_1 = \varepsilon_{11}, \varepsilon_2 = \varepsilon_{22}, \varepsilon_3 = \varepsilon_{33}, \varepsilon_4 = 2\varepsilon_{23}, \varepsilon_5 = 2\varepsilon_{31}, \varepsilon_6 = 2\varepsilon_{12} \tag{3.121}$$

For an orthotropic lamina, it is assumed that $\sigma_3 = 0$. Thus, Eq. 3.118 can be rewritten as:

$$\varepsilon_3 = S_{13}\sigma_1 + S_{23}\sigma_2 \tag{3.122}$$

$$\begin{Bmatrix}\varepsilon_1\\ \varepsilon_2\\ \varepsilon_6\end{Bmatrix} = \begin{bmatrix}S_{11} & S_{12} & 0\\ S_{12} & S_{22} & 0\\ 0 & 0 & S_{66}\end{bmatrix}\begin{Bmatrix}\sigma_1\\ \sigma_2\\ \sigma_6\end{Bmatrix} \tag{3.123}$$

$$\begin{Bmatrix}\varepsilon_4\\ \varepsilon_5\end{Bmatrix} = \begin{bmatrix}S_{44} & 0\\ 0 & S_{55}\end{bmatrix}\begin{Bmatrix}\sigma_4\\ \sigma_5\end{Bmatrix} \tag{3.124}$$

and the stress-strain relationship can be written as:

$$\begin{Bmatrix}\sigma_1\\ \sigma_2\\ \sigma_6\end{Bmatrix} = \begin{bmatrix}Q_{11} & Q_{12} & 0\\ Q_{12} & Q_{22} & 0\\ 0 & 0 & Q_{66}\end{bmatrix}\begin{Bmatrix}\varepsilon_1\\ \varepsilon_2\\ \varepsilon_6\end{Bmatrix} \tag{3.125}$$

$$\begin{Bmatrix}\sigma_4\\ \sigma_5\end{Bmatrix} = \begin{bmatrix}Q_{44} & 0\\ 0 & Q_{55}\end{bmatrix}\begin{Bmatrix}\varepsilon_4\\ \varepsilon_5\end{Bmatrix} \tag{3.126}$$

where Q_{ij} is:

$$Q_{11} = \frac{E_1}{1 - \nu_{12}\nu_{21}} \tag{3.127}$$

$$Q_{22} = \frac{E_2}{1 - \nu_{12}\nu_{21}}$$

$$Q_{12} = \frac{\nu_{12}E_2}{1 - \nu_{12}\nu_{21}}$$

$$Q_{44} = G_{23}, Q_{55} = G_{31}, Q_{66} = G_{12}$$

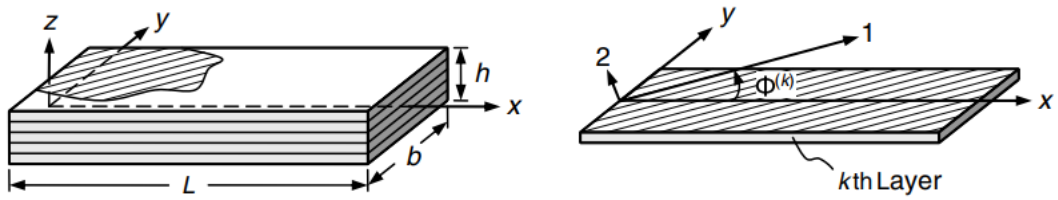

Figure 3.26: Global and local coordinates on a lamina [Lee, 2009]

Assuming that the local coordinates on a lamina shown by axes (1-2) in Figure 3.26 on the right, are obtained by rotating the x-y-z global coordinates on the left around the z axis counterclockwise by an angle of $\phi^{(k)}$, the coordinate transformation rules are derived as follows:

$$\begin{Bmatrix}\sigma_{xx}\\ \sigma_{yy}\\ \sigma_{xy}\end{Bmatrix} = \begin{bmatrix}\cos^2\phi & \sin^2\phi & -sin2\phi\\ \sin^2\phi & \cos^2\phi & sin2\phi\\ sin\phi cos\phi & -sin\phi cos\phi & \cos^2\phi-\sin^2\phi\end{bmatrix}\begin{Bmatrix}\sigma_1\\ \sigma_2\\ \sigma_6\end{Bmatrix} \tag{3.128}$$

$$\begin{Bmatrix}\sigma_{yz}\\ \sigma_{zx}\end{Bmatrix} = \begin{bmatrix}cos\phi & sin\phi\\ -sin\phi & cos\phi\end{bmatrix}\begin{Bmatrix}\sigma_4\\ \sigma_5\end{Bmatrix} \tag{3.129}$$

and:

$$\begin{Bmatrix}\varepsilon_{xx}\\ \varepsilon_{yy}\\ \varepsilon_{xy}\end{Bmatrix} = \begin{bmatrix}\cos^2\phi & \sin^2\phi & -sin2\phi\\ \sin^2\phi & \cos^2\phi & sin2\phi\\ sin\phi cos\phi & -sin\phi cos\phi & \cos^2\phi-\sin^2\phi\end{bmatrix}\begin{Bmatrix}\varepsilon_1\\ \varepsilon_2\\ \varepsilon_6\end{Bmatrix} \tag{3.130}$$

$$\begin{Bmatrix}\gamma_{yz}\\ \gamma_{zx}\end{Bmatrix} = \begin{bmatrix}cos\phi & sin\phi\\ -sin\phi & cos\phi\end{bmatrix}\begin{Bmatrix}\varepsilon_4\\ \varepsilon_5\end{Bmatrix} \tag{3.131}$$

By applying the above relations into Eq. 3.125 and Eq. 3.126, the stress-strain relationships with respect to the global coordinates are obtained as:

$$\begin{Bmatrix}\sigma_{xx}\\ \sigma_{yy}\\ \sigma_{xy}\end{Bmatrix} = \begin{bmatrix}\bar{Q}_{11} & \bar{Q}_{12} & \bar{Q}_{16}\\ \bar{Q}_{12} & \bar{Q}_{22} & \bar{Q}_{26}\\ \bar{Q}_{16} & \bar{Q}_{26} & \bar{Q}_{66}\end{bmatrix}\begin{Bmatrix}\varepsilon_{xx}\\ \varepsilon_{yy}\\ \gamma_{xy}\end{Bmatrix} \tag{3.132}$$

$$\begin{Bmatrix}\sigma_{yz}\\ \sigma_{zx}\end{Bmatrix} = \begin{bmatrix}\bar{Q}_{44} & \bar{Q}_{45}\\ \bar{Q}_{45} & \bar{Q}_{55}\end{bmatrix}\begin{Bmatrix}\gamma_{yz}\\ \gamma_{zx}\end{Bmatrix} \tag{3.133}$$

where $\bar{Q}_{ij}$ are calculated as:

$$\bar{Q}_{11} = Q_{11}\cos^4\phi + Q_{22}\sin^4\phi + 2(Q_{12} + 2Q_{66})\sin^2\phi\cos^2\phi \quad (3.134)$$

$$\bar{Q}_{22} = Q_{11}sin^4\phi + Q_{22}\cos^4\phi + 2(Q_{12} + 2Q_{66})\sin^2\phi\cos^2\phi$$

$$\bar{Q}_{66} = Q_{66}(sin^4\phi + \cos^4\phi) + (Q_{11} + Q_{22} - 2Q_{12} - 2Q_{66})\sin^2\phi\cos^2\phi$$

$$\bar{Q}_{12} = Q_{12}(sin^4\phi + \cos^4\phi) + (Q_{11} + Q_{22} - 4Q_{66})\sin^2\phi\cos^2\phi$$

$$\bar{Q}_{16} = (Q_{11} - Q_{12} - 2Q_{66})sin\phi\cos^3\phi + (Q_{12} - Q_{22} + 2Q_{66})\sin^3\phi\, cos\phi$$

$$\bar{Q}_{26} = (Q_{11} - Q_{12} - 2Q_{66})\sin^3\phi\, cos\phi + (Q_{12} - Q_{22} + 2Q_{66})sin\phi\cos^3\phi$$

$$\bar{Q}_{44} = Q_{44}\cos^2\phi + Q_{55}\sin^2\phi, \bar{Q}_{55} = Q_{55}\cos^2\phi + Q_{44}\sin^2\phi$$

$$\bar{Q}_{45} = (Q_{55} - Q_{44})cos\phi sin\phi$$

Assume that $u, v, and\ w$ represent the displacements in x-, y- and z-directions, respectively. u_0 and w_0 are the displacements of a point on the reference plane, located on the midplane of the beam with $z = 0$, in the x- and z-directions, and θ_y and θ_z are the negative of the rotations around the y- and z-axes, respectively. The displacements are written as:

$$u(x, y, z, t) = u_0(x, y, t) - z\theta_y(x, y, t) \quad (3.135)$$

$$v(x, y, z, t) = -z\theta_z(x, y, t) \quad (3.136)$$

$$w(x, y, z, t) = w_0(x, y, t) \quad (3.137)$$

$u, v, and\ w$

Strains in the x-y-z directions can be written as:

$$\varepsilon_{xx} = \frac{\partial u}{\partial x} \quad (3.138)$$

$$\varepsilon_{yy} = \frac{\partial v}{\partial y} \quad (3.139)$$

$$\gamma_{xy} = \frac{\partial v}{\partial x} + \frac{\partial u}{\partial y} \quad (3.140)$$

$$\gamma_{yz} = \frac{\partial w}{\partial y} + \frac{\partial v}{\partial z} \quad (3.141)$$

$$\gamma_{zx} = \frac{\partial w}{\partial x} + \frac{\partial u}{\partial z} \quad (3.142)$$

Substituting Eq. 3.135 – Eq. 3.137 in Eq. 3.138 – Eq.3.142 gives:

$$\varepsilon_{xx} = \frac{\partial u_0}{\partial x} - z\frac{\partial \theta_y}{\partial x} \tag{3.143}$$

$$\varepsilon_{yy} = -z\frac{\partial \theta_z}{\partial y} \tag{3.144}$$

$$\gamma_{xy} = \frac{\partial u_0}{\partial y} - z\left(\frac{\partial \theta_z}{\partial x} + \frac{\partial \theta_y}{\partial y}\right) \tag{3.145}$$

$$\gamma_{yz} = \frac{\partial w_0}{\partial y} - \theta_z \tag{3.146}$$

$$\gamma_{zx} = \frac{\partial w_0}{\partial x} - \theta_y \tag{3.147}$$

The resulting forces and moments can be calculated by integrating stresses through the laminate thickness, where N_x is the internal axial force per unit width, V_x is the shear force per unit width, M_{xx} is the bending moment around the x-axis per unit width, M_{yy} is the bending moment around y axis per unit width and M_{xy} is the twisting moment per unit width. b is the width of the laminate, h is the thickness of the beam and κ is the shear correction factor. N is the number of layers and z_k is shown in Figure 3.27.

$$\begin{Bmatrix} N_x \\ V_x \end{Bmatrix} = \int_{-\frac{h}{2}}^{\frac{h}{2}} \begin{Bmatrix} \sigma_{xx} \\ \kappa\sigma_{zx} \end{Bmatrix} dz = \sum_{k=1}^{N} \int_{z_{k-1}}^{z_k} \begin{Bmatrix} {\sigma_{xx}}^{(k)} \\ \kappa{\sigma_{zx}}^{(k)} \end{Bmatrix} dz \tag{3.148}$$

$$\begin{Bmatrix} M_{xx} \\ M_{yy} \\ M_{xy} \end{Bmatrix} = \int_{-\frac{h}{2}}^{\frac{h}{2}} \begin{Bmatrix} \sigma_{xx} \\ \sigma_{yy} \\ \sigma_{xy} \end{Bmatrix} z dz = \sum_{k=1}^{N} \int_{z_{k-1}}^{z_k} \begin{Bmatrix} {\sigma_{xx}}^{(k)} \\ {\sigma_{yy}}^{(k)} \\ {\sigma_{xy}}^{(k)} \end{Bmatrix} z dz \tag{3.149}$$

Using the stress-strain relation of a lamina in Eq. 3.132 and Eq. 3.133, internal forces and moments are obtained as:

$$N_x = A_{11}\frac{\partial u_0}{\partial x} + A_{11}\frac{\partial u_0}{\partial y} + B_{11}\left(-\frac{\partial \theta_y}{\partial x}\right) + B_{12}\left(-\frac{\partial \theta_z}{\partial y}\right) - B_{16}\left(\frac{\partial \theta_z}{\partial x} + \frac{\partial \theta_y}{\partial y}\right) \tag{3.150}$$

$$V_x = \kappa A_{45}\left(\frac{\partial w_0}{\partial y} - \theta_z\right) + \kappa A_{55}\left(\frac{\partial w_0}{\partial x} - \theta_y\right) \tag{3.151}$$

$$\begin{Bmatrix} M_{xx} \\ M_{yy} \\ M_{xy} \end{Bmatrix} = \begin{bmatrix} B_{11} & B_{16} \\ B_{12} & B_{26} \\ B_{16} & B_{66} \end{bmatrix} \begin{Bmatrix} \frac{\partial u_0}{\partial x} \\ \frac{\partial u_0}{\partial y} \end{Bmatrix} + \begin{bmatrix} D_{11} & D_{12} & D_{16} \\ D_{12} & D_{22} & D_{26} \\ D_{16} & D_{26} & D_{66} \end{bmatrix} \begin{Bmatrix} -\frac{\partial \theta_y}{\partial x} \\ -\frac{\partial \theta_z}{\partial y} \\ -(\frac{\partial \theta_z}{\partial x} + \frac{\partial \theta_y}{\partial y}) \end{Bmatrix} \tag{3.152}$$

where:

$$A_{ij} = \sum_{k=1}^{N} \bar{Q}_{ij}{}^{(k)} \left(z_k - z_{k-1} \right) \tag{3.153}$$

$$B_{ij} = \frac{1}{2}\sum_{k=1}^{N} \bar{Q}_{ij}{}^{(k)} \left(z_k^2 - z_{k-1}^2 \right) \tag{3.154}$$

$$D_{ij} = \frac{1}{3}\sum_{k=1}^{N} \bar{Q}_{ij}{}^{(k)} \left(z_k^3 - z_{k-1}^3 \right) \tag{3.155}$$

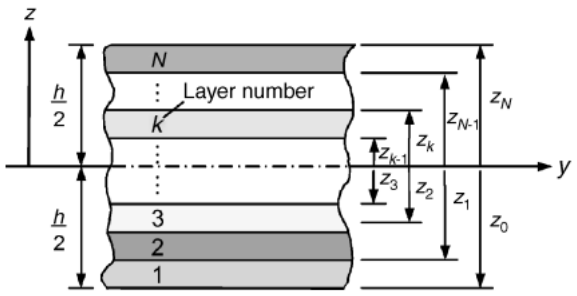

Figure 3.27: Geometry of laminate (x axis is out of plane)

For a beam, it is assumed that the transverse displacement is constant along the thickness as shown in Eq. 3.156.

$$w(x, y, z, t) = w_0(x, t) \tag{3.156}$$

Axial displacement is only a function of longitudinal direction (x-direction) and y-direction does not affect that as shown in Eq. 3.157.

$$u(x, y, z, t) = u_0(x, t) - z\theta(x, t) \tag{3.157}$$

No rotation is assumed in the y-direction and the only assumed rotation is around the x-direction as shown in Eq. 3.158 and Eq. 3.159.

$$\theta_y = \theta \tag{3.158}$$

$$\theta_z = 0 \tag{3.159}$$

Substituting Eq. 3.159 in Eq. 3.136 gives:

$$v(x, y, z, t) = 0 \tag{3.160}$$

Applying Eq. 3.156-3.160 in the strain relationships gives:

$$\varepsilon_{yy} = 0 \tag{3.161}$$

$$\gamma_{xy} = \left(\frac{\partial \theta_z}{\partial x} + \frac{\partial \theta_y}{\partial y}\right) = 0 \tag{3.162}$$

The following changes in notations are defined to make equations more compact:

$$\frac{\partial \theta_y}{\partial x} = \theta' \tag{3.163}$$

$$\frac{\partial u_0}{\partial x} = u_0' \tag{3.164}$$

Substituting the new notations for strains in Eq. 3.150-3.152 gives the equations below for the forces and moments:

$$N(x, t) = bN_x = bA_{11}u_0' - bB_{11}\theta' \tag{3.165}$$

$$V(x, t) = bQ_x = \mathrm{b}\kappa A_{55}(w_0' - \theta) \tag{3.166}$$

$$M(x, t) = bM_{xx} = bD_{11}\theta' - bB_{11}u_0' \tag{3.167}$$

bA_{11} is the axial rigidity, bB_{11} is coupled axial-bending rigidity, $\mathrm{b}\kappa A_{55}$ is shear rigidity, and bD_{11} is bending rigidity.

The equations of motion and associated boundary conditions for composite beams are derived from Hamilton's principle based on the first-order shear deformation theory.

$$\int_0^t (\delta T - \delta U + \delta W)dt = 0 \tag{3.168}$$

where δT is the variation of the kinetic energy, δU is the variation of the potential energy and δW is the variation of the work of the external forces. The sign convention used for the composite laminate beam is shown in Figure 3.28.

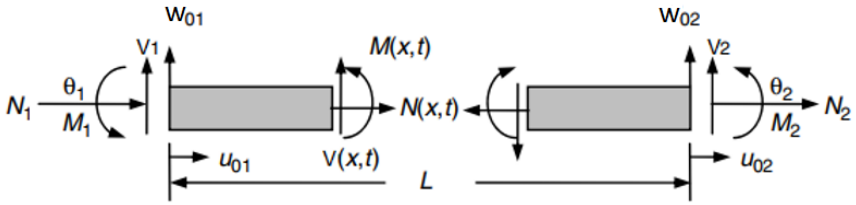

Figure 3.28: Internal forces and moments

Potential energy can be written as

$$\mathrm{U} = \frac{1}{2}\int_0^L \{ Nu_0' + M\theta' + \mathrm{V}(w_0' - \theta) \}dx = \frac{1}{2}\int_0^L \{ bA_{11}{u_0'}^2 - 2\mathrm{b}B_{11}\theta' u_0' + \mathrm{b}D_{11}{\theta'}^2 + \mathrm{b}\kappa A_{55}(w_0' - \theta)^2 \}\, dx \tag{3.169}$$

Kinetic energy is written as:

$$\mathrm{T} = \frac{1}{2}\int_0^L \int_{-\frac{h}{2}}^{\frac{h}{2}} \{\rho \mathrm{b}\,(\dot{w}^2 + \dot{u}^2)\}\mathrm{d}z\,dx = \frac{1}{2}\int_0^L [\int_{-\frac{h}{2}}^{\frac{h}{2}} \rho \mathrm{b}\,(\dot{w}_0^2)dz + \int_{-\frac{h}{2}}^{\frac{h}{2}} \rho \mathrm{b}\,(\dot{u}_0^2)dz]dx \tag{3.170}$$

$$T = \frac{1}{2}\int_0^L [\,\dot{w}_0^2 I_0 + \dot{u}_0^2 I_0 + \dot{\theta}^2 I_2 - 2\dot{\theta}\dot{u}_0 I_1]dx \tag{3.171}$$

I_0, I_1, I_2 represent mass per unit length, first-order mass moment of inertia per unit length and second-order mass moment of inertia per unit length.

$$I_0 = \int_{-\frac{h}{2}}^{\frac{h}{2}} \rho \mathrm{b}dz \tag{3.172}$$

$$I_1 = \int_{-\frac{h}{2}}^{\frac{h}{2}} \rho b z dz$$

$$I_2 = \int_{-\frac{h}{2}}^{\frac{h}{2}} \rho b z^2 dz$$

Variations of U and T are calculated according to Eq 3.173 and Hamilton's principle introduced in Eq. 3.168 is used as shown in Eq. 3.174:

$$\delta F(y, y', x) = \left[\frac{\partial F}{\partial y} - \frac{d}{dx}\left(\frac{\partial F}{\partial y'}\right)\right] \delta y \tag{3.173}$$

$$\int_0^t (\delta T - \delta U + \delta W) dt = \tag{3.174}$$

$$\int_0^t [\int_0^l \{ [b\kappa A_{55} (w_0'' - \theta') - I_0 \ddot{w}_0] \delta w_0 + [bD_{11} \theta''^2 + bA_{55}(w_0' - \theta) - bB_{11} u_0'' + I_1 \ddot{u}_0 - I_2 \ddot{\theta}] \delta\theta + \left[bA_{11} u_0'' - bB_{11} \theta'' - I_0 \ddot{u}_0 + I_1 \ddot{\theta}\right] \delta u_0 \} dx - N(x,t) \delta u_0 |_0^L - M(x,t) \delta\theta |_0^L - V(x,t) \delta w_0 |_0^L + N_1 \delta u_0(0) + N_2 \delta u_0(L) + M_1 \delta\theta(0) + M_2 \delta\theta(L) + V_1 \delta w_0(0) + V_2 \delta w_0(L)] dt = 0$$

The equations of motion are derived from Eq 3.174 as:

$$bA_{11} u_0'' - bB_{11} \theta'' - I_0 \ddot{u}_0 + I_1 \ddot{\theta} = 0 \tag{3.175}$$

$$b\kappa A_{55}(w_0'' - \theta') - I_0 \ddot{w}_0 = 0 \tag{3.176}$$

$$bD_{11} \theta''^2 + bA_{55}(w_0' - \theta) - bB_{11} u_0'' + I_1 \ddot{u}_0 - I_2 \ddot{\theta} = 0 \tag{3.177}$$

For a laminated beam with mid-plane symmetry, B_{11} and I_1 are equal to zero. In that case, Eq. 3.175 is equivalent to axial vibration of a bar and Eq. 3.176 and Eq. 3.177 are the differential equations of motion of the Timoshenko beam element. This means that for the case of a laminated beam with mid-plane symmetry, the axial vibration is decoupled from the shear-bending vibration.

If the shear deformation is assumed to be negligible, then the Euler-Bernoulli beam element developed in section 3.4 plus the axial bar element in section 3.2 can be used together to capture the vibration of a laminated beam with mid-plane symmetry. The term bD_{11} is the bending stiffness

and is equivalent to the term EI used in the isotropic Euler-Bernoulli beam element. The term bA_{11} is the axial stiffness and is equivalent to the term EA used in bar element.

3.21. Modeling delamination using Multiple Point Constraints (MPC)

The idea used to model delamination in this study is close to what was used in [Pardoen and Tracy, 1997]. The sub-laminates above and below the delamination are treated as two beams separated from the base-laminate. The effect of micromechanics and surface friction is not considered in this modeling and the delamination is assumed to cover the entire width of the composite beam. The entire length of the delaminated area is covered by adding three extra beam/spectral elements (the sub-laminates) and 6 extra nodes. This simplifying assumption helps with reducing the computational effort which is the main concern in inverse problems [Nag et al, 2002]. Each of the sub-laminates and base-laminates are considered together as a structural wave guide.

The location of the nodes of the spectral elements for a delaminated beam is shown in Figure 3.29. In the absence of delamination, one spectral element between node 1 and node 4 is enough. However, the presence of delamination requires having 3 more elements and 6 more nodes. Six more nodes are added to model base-laminates and sub-laminates. The sub-laminate element nodes are located at the mid-plane of the sub-laminates.

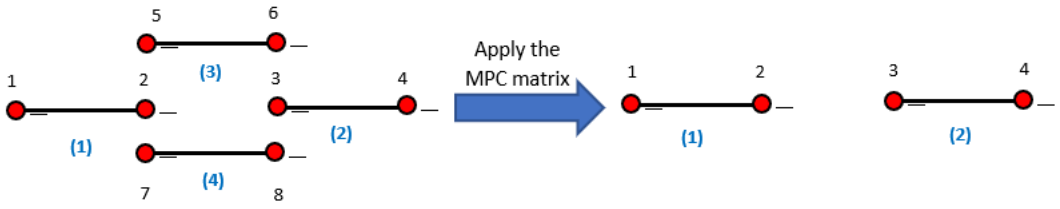

Figure 3.29: Delamination modeling using MPC

The kinematic assumption for the interface of base-laminate and sub-laminate is that the cross-section remains plane and the slope is continuous and constant at the interface. This assumption can be written in the following format:

$$\begin{Bmatrix} u_5 \\ v_5 \\ \theta_5 \end{Bmatrix} = \begin{Bmatrix} u_2 + \frac{h}{2}\theta_2 \\ v_2 \\ \theta_2 \end{Bmatrix}, \qquad \begin{Bmatrix} u_7 \\ v_7 \\ \theta_7 \end{Bmatrix} = \begin{Bmatrix} u_2 - \frac{h}{2}\theta_2 \\ v_2 \\ \theta_2 \end{Bmatrix} \tag{3.178}$$

and:

$$\begin{Bmatrix} u_6 \\ v_6 \\ \theta_6 \end{Bmatrix} = \begin{Bmatrix} u_3 + \frac{h}{2}\theta_3 \\ v_3 \\ \theta_3 \end{Bmatrix}, \qquad \begin{Bmatrix} u_8 \\ v_8 \\ \theta_8 \end{Bmatrix} = \begin{Bmatrix} u_3 - \frac{h}{2}\theta_3 \\ v_3 \\ \theta_3 \end{Bmatrix} \tag{3.179}$$

In Eq 3.178 and 3.179, h is the height of the beam. Nodes 2 and 3 are called master nodes and nodes 5, 6, 7, and 8 are called slave nodes meaning that their degrees of freedom depend on the degrees of freedom of the master nodes. Considering the relationship between the master nodes and the slave nodes, assuming that $\{\boldsymbol{d}\}$ contains the degrees of freedom the structure on the left in Figure 3.29 and $\{\boldsymbol{d}_r\}$ contains the degrees of freedom of the structure on the right in Figure 3.29, $\{\boldsymbol{d}\}$ and $\{\boldsymbol{d}_r\}$ are related to each other using Eq. 3.180:

$$[\boldsymbol{C}]^T\{\boldsymbol{d}\} = \{\boldsymbol{d}_r\} \tag{3.180}$$

Table 3.1: Entries of the [**C**] matrix

	u1	v1	theta1	u2	v2	theta2	u3	v3	theta3	u4	v4	theta4
u1	1	0	0	0	0	0	0	0	0	0	0	0
v1	0	1	0	0	0	0	0	0	0	0	0	0
theta1	0	0	1	0	0	0	0	0	0	0	0	0
u2	0	0	0	1	0	0	0	0	0	0	0	0
v2	0	0	0	0	1	0	0	0	0	0	0	0
theta2	0	0	0	0	0	1	0	0	0	0	0	0
u3	0	0	0	0	0	0	1	0	0	0	0	0
v3	0	0	0	0	0	0	0	1	0	0	0	0
theta3	0	0	0	0	0	0	0	0	1	0	0	0
u4	0	0	0	0	0	0	0	0	0	1	0	0
v4	0	0	0	0	0	0	0	0	0	0	1	0
theta4	0	0	0	0	0	0	0	0	0	0	0	1
u5	0	0	0	1	0	$\frac{h}{2}$	0	0	0	0	0	0
v5	0	0	0	0	1	0	0	0	0	0	0	0
theta5	0	0	0	0	0	1	0	0	0	0	0	0
u6	0	0	0	1	0	$-\frac{h}{2}$	0	0	0	0	0	0
v6	0	0	0	0	1	0	0	0	0	0	0	0
theta6	0	0	0	0	0	1	0	0	0	0	0	0
u7	0	0	0	0	0	0	1	0	$\frac{h}{2}$	0	0	0
v7	0	0	0	0	0	0	0	1	0	0	0	0
theta7	0	0	0	0	0	0	0	0	1	0	0	0
u8	0	0	0	0	0	0	1	0	$-\frac{h}{2}$	0	0	0
v8	0	0	0	0	0	0	0	1	0	0	0	0
theta8	0	0	0	0	0	0	0	0	1	0	0	0

The entries of $[\boldsymbol{C}]_{24\times12}$ are obtained from Table 3.1. Rows of this table correspond to degrees of freedom in $\{\boldsymbol{d}\}$ and the columns correspond to the degrees of freedom in $\{\boldsymbol{d}_r\}$. Consequently, the global dynamic stiffness matrix can be obtained as in Eq. 3.181:

$$[\boldsymbol{K}(\omega)]^{MPC} = [\boldsymbol{C}]^T[\boldsymbol{K}(\omega)][\boldsymbol{C}] \tag{3.181}$$

3.22. Modeling for contact in the delaminated area

The effect of distributed contact between the delaminated surfaces was not considered in the formulation in section 3.21. The objective of this section is to add the additional effect due to the distributed contact at the delaminated zone comprising of contact of chopped fibers and matrix [Nag et al, 2003].

Conventional spring elements with stiffnesses in both X and Y directions are used to connect the top and bottom layers in the delaminated zone. The stiffness matrix of this element is shown in Eq. 3.182.

$$K_{spring} = \begin{bmatrix} K_x & 0 & 0 & -K_x & 0 & 0 \\ 0 & K_y & 0 & 0 & -K_y & 0 \\ 0 & 0 & 0 & 0 & 0 & 0 \\ -K_x & 0 & 0 & K_x & 0 & 0 \\ 0 & -K_y & 0 & 0 & K_y & 0 \\ 0 & 0 & 0 & 0 & 0 & 0 \end{bmatrix} \tag{3.182}$$

K_x and K_y denote the stiffnesses of the spring element in X and Y directions, respectively. Determining the exact stiffness of this matrix is beyond the scope of this thesis. However, the spring elements can represent the behavior of chopped fibers between the top and bottom layers and their values can be an approximation of the axial stiffness of the fibers. It will be shown that by increasing the number of elements in the delaminated area and increasing their stiffness, the behavior of the delaminated beams gets closer to the fully bonded model (The result of this case study will be discussed in Chapter 4). Thus, this approach can be used to model the behavior between the fully delaminated and fully bonded case which will be closer to what happens in a real case.

Although use of many elements in the delaminated zone to capture the distributed contact undermines to some extent the idea of use of spectral elements to avoid mesh refinement, the author believes it might be possible to add a spectral truss element to capture the behavior of the distributed contact zone with only one spectral element.

3.23. Computer implementation

The methodology described in this chapter is implemented as two computer programs connected to each other. The Spectral Finite Element analysis program is written in FORTRAN using Intel FORTRAN Compiler integrated into Microsoft Visual Studio Compiler. Program reads input data such as material properties, boundary conditions and number of elements from input test files and stores the output, such as response of a selected degree-of-freedom and natural frequencies and mode shapes in separate text files. The flowchart in Figure 3.30 shows the steps taken in this program.

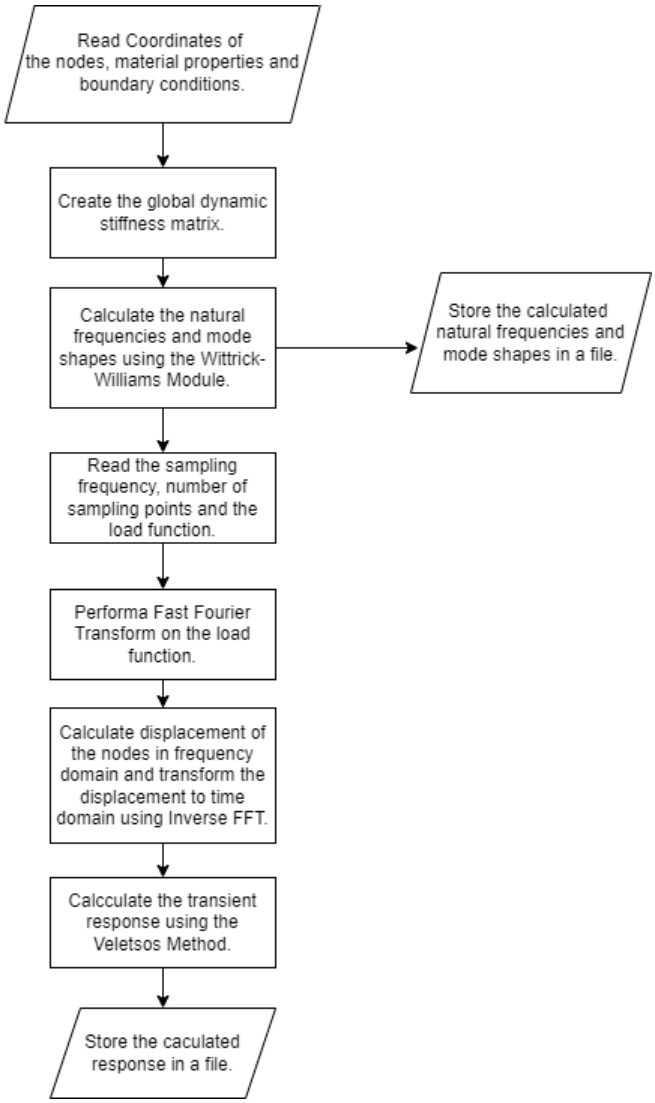

Figure 3.30: Flowchart of the Spectral Finite Element program written in FORTRAN

The damage detection algorithm is written in Python using the Jupyter Notebook environment. It uses the FORTRAN program to calculate natural frequencies and mode shapes of possible damage cases. The flow chart in Figure 3.31 shows the steps taken in the damage detection program.

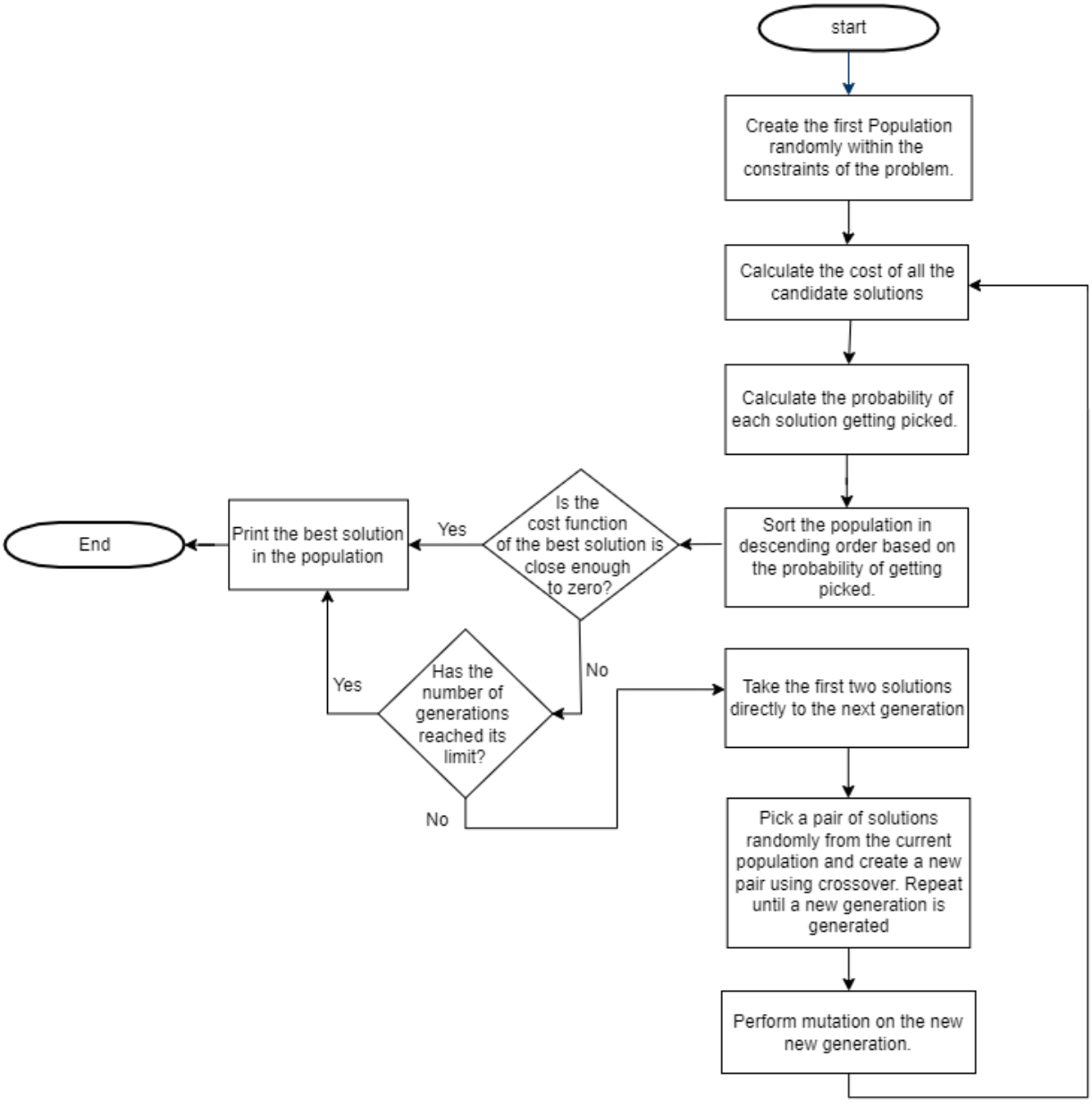

Figure 3.31: Flowchart of the damage detection program written in Python

Chapter 4

Case studies

4.1. Natural frequencies of Euler-Bernoulli beams using Spectral Finite Element and Wittrick-Williams method

Consider the simply-supported beam shown in Figure 3.10. To calculate the natural frequencies and vibration mode shapes, the beam is modelled once with spectral elements and another time with conventional finite elements. The Wittrick-Williams method is applied to the spectral element model and linear eigenvalue analysis is applied to the finite element model.

Table 4.1: Natural frequencies of the simply-supported beam in Figure 3.10

Bending mode Number	Analytical (Hz)	Finite Element [2 Elements] (Hz)	Finite Element [3 Elements] (Hz)	Finite Element [4 Elements] (Hz)	Finite Element [5 Elements] (Hz)	Spectral Element [2 Elements] (Hz)
1	31.24	31.36	31.26	31.24	31.24	31.24
2	124.95	138.68	126.42	125.44	125.15	124.95
3	281.13	348.58	312.03	286.27	283.36	281.13
4	499.79	635.51	580.2	554.72	511.3	499.79

The results of the modeling explained above are compared with the analytical results and shown in Table 4.1 and Table 4.2. As shown in Table 4.1, by increasing the number of elements in a conventional finite element model, results converge to the analytical solution. However, it is shown in Figure 4.1 that the convergence rate drops as the mode number increases. On the other hand, the spectral finite element model captures the exact frequency of all the first four modes with only 2 spectral elements.

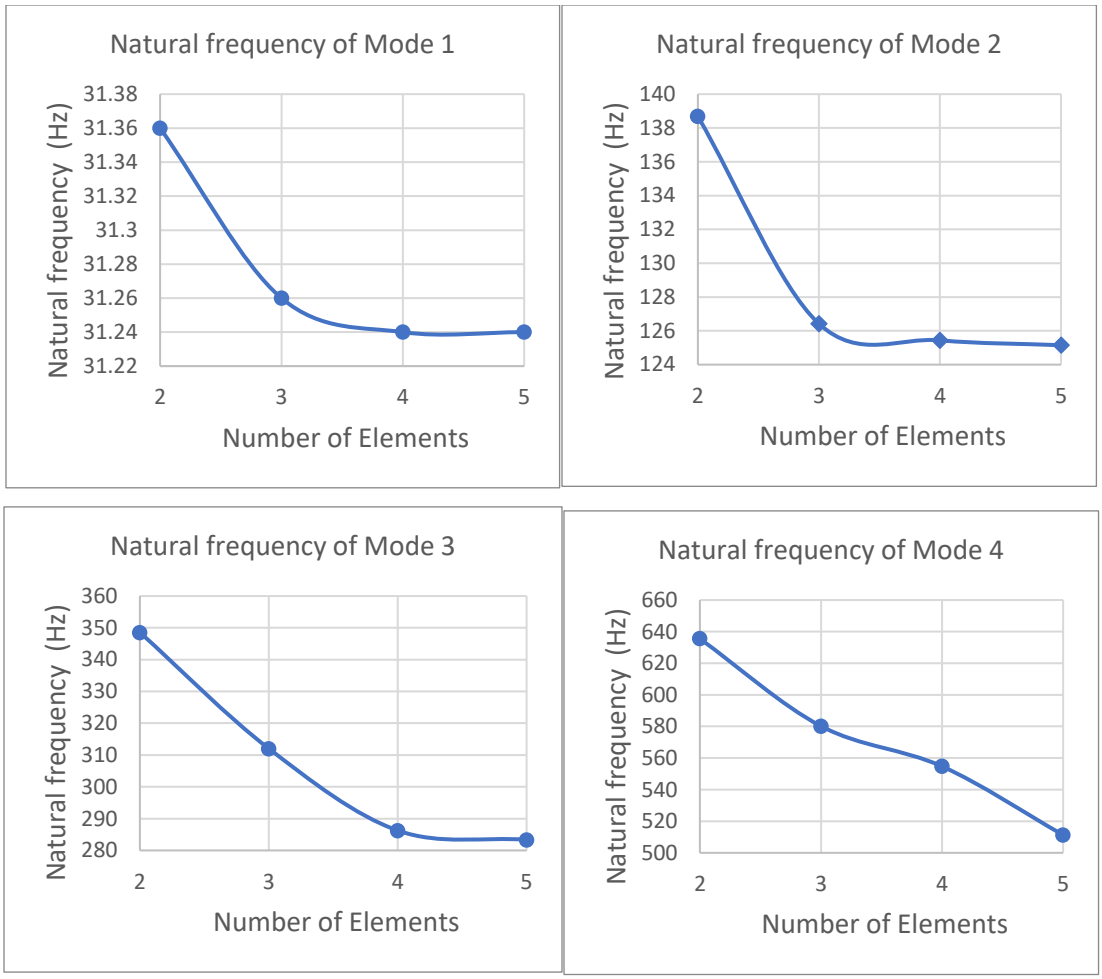

Figure 4.1:Effect of mesh refinement on natural frequencies obtained by conventional Finite Element Method

4.2. Vibration mode shapes of Euler-Bernoulli beams using Spectral Finite Element and Wittrick-Williams method

As explained in section 3.11, the method proposed by [Veletsos and Kumar, 1983] was suggested to construct the transient response based on the steady-state response. The method requires having access to natural frequencies and the corresponding modes of vibration. Using the Wittrick-Williams method explained in section 3.12, the natural frequencies of the structure up to any desired value are obtained. To calculate the corresponding modes of vibration, the free vibration equation of motion, $[K(\omega)]\{d\} = 0$, is used. Two spectral beam elements are used to model the beam shown in Figure 3.10. The model used is shown in Figure 4.2.

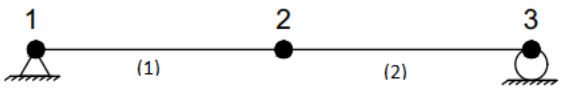

Figure 4.2: Spectral Finite Element model of the beam shown in Figure 3.10

Table 4.2: Mode shapes calculated by the Spectral Finite Element model

	Mode 1		Mode 2		Mode 3	
Degree of freedom	Spectral Element	Analytical Solution	Spectral Element	Analytical Solution	Spectral Element	Analytical Solution
v_1	0	0	0	0	0	0
θ_1	-1	-1	1	1	-1	-1
v_2	-19.10	-19.10	0	0	6.37	6.37
θ_2	0	0	-1	-1	0	0
v_3	0	0	0	0	0	0
θ_3	1	1	1	1	1	1

The first three mode shapes obtained from the spectral element model are compared with the analytical solution. A spectral finite element model with 2 elements is used. The results are shown in Table 4.2 and it is observed that the mode shapes obtained by the spectral element model are very close to the analytical solution at the nodes.

4.3. Complete response of Euler-Bernoulli beam under dynamic load using SFEM [Veletsos and Kumar, 1983]

According to Eq. 3.102 in section 3.11, the complete response of the structure can be obtained using the steady-state response, natural frequencies and mode shapes of vibration. The mass matrix in Eq 3.102, is assumed to be a lumped mass matrix with the mass matrix shown in Eq. 4.1:

$$[\boldsymbol{M}] = \rho AL \begin{bmatrix} 0.5 & 0 & 0 & 0 \\ 0 & 0 & 0 & 0 \\ 0 & 0 & 0.5 & 0 \\ 0 & 0 & 0 & 0 \end{bmatrix} \tag{4.1}$$

where ρ is the density of the material, A is the cross-section of the beam and L is the length of the beam element.

Transverse displacements of the middle point of the beam shown in Figure 3.10 under the force functions shown in Figure 3.11 are calculated by using the first mode of vibration in Eq. 3.102 and are shown in Figure 4.3:

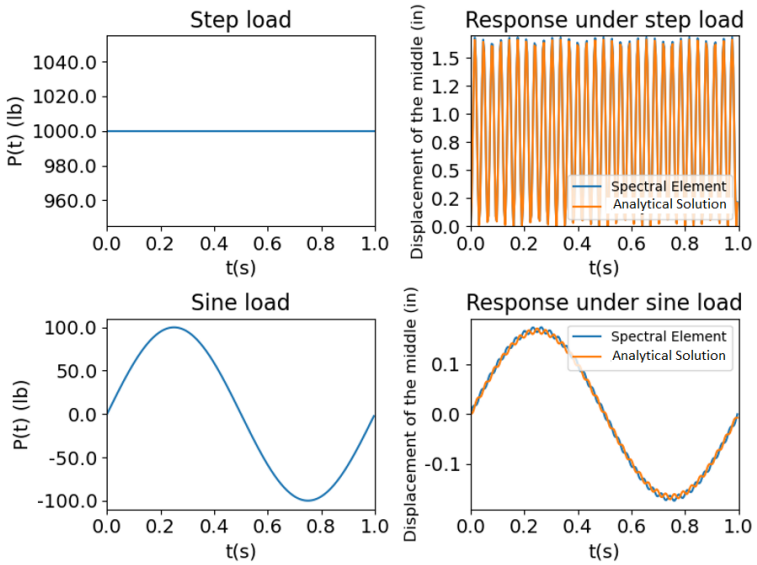

Figure 4.3: Complete transverse displacement of the beam under concentrated transverse load applied at the middle point.

4.4. Natural frequencies of Laminated Composite beam using Spectral Finite Element and Wittrick-Williams method

As discussed in section 3.20, vibration of a laminated composite beam which is symmetric about its mid-plane, can be modeled as uncoupled vibrations of a beam element and a bar element. For this purpose, the spectral beam and spectral bar elements introduced in chapter 3 are combined to create a spectral frame element with axial, transverse and rotational degrees of freedom at each node as shown in Figure 4.4. The dynamic stiffness matrix of this element is written as Eq. 4.2. In this equation, K_{ij}^{bar} is the j^{th} element on the i^{th} row of the stiffness matrix of the spectral bar element introduced in Eq. 3.12 and K_{ij}^{beam} is the j^{th} element on the i^{th} row of the stiffness matrix of the spectral beam element introduced in Eq. 3.47.

$$[\boldsymbol{K}^{frame}(\omega)] = \begin{bmatrix} K_{11}^{bar} & 0 & 0 & K_{12}^{bar} & 0 & 0 \\ 0 & K_{11}^{beam} & K_{12}^{beam} & 0 & K_{13}^{beam} & K_{14}^{beam} \\ 0 & K_{21}^{beam} & K_{22}^{beam} & 0 & K_{23}^{beam} & K_{24}^{beam} \\ K_{21}^{bar} & 0 & 0 & K_{22}^{bar} & 0 & 0 \\ 0 & K_{31}^{beam} & K_{32}^{beam} & 0 & K_{33}^{beam} & K_{34}^{beam} \\ 0 & K_{41}^{beam} & K_{42}^{beam} & 0 & K_{43}^{beam} & K_{44}^{beam} \end{bmatrix} \tag{4.2}$$

Figure 4.4: Frame element

Example 1:

[Okafor et al, 1996] conducted experimental and numerical studies to investigate the effect of delamination on modal frequencies of Glass/epoxy composite beams. Modal frequencies were obtained using modal testing. Polyvinylidene fluoride film (PVDF) was used to measure dynamic strain signal and the beam was excited using an instrumented hammer and a piezoceramic patch.

Test specimens of laminated beams were obtained from an eight-ply $[0^{\circ}/90^{\circ}/90^{\circ}/0^{\circ}]_s$ glass/epoxy laminate. Material properties of the ply are:

$E_1 = 42.34\ GPa, \quad E_2 = 11.72\ GPa, \quad G_{12} = 1.67 \times 10^{10} Pa,\ G_{13} = 1.67 \times 10^{10} Pa,\ G_{23} = 5.47 \times 10^{9} Pa,\ \nu_{12} = 0.27, \rho = 1901.5 \frac{kg}{m^3}$

The composite laminate is 26.67 cm long, 2.54 cm wide and 0.1788 cm thick.

An instrumented hammer was used to excite the beam and a PVDF sensor was used to measure the response. The beam was studied under Clamped-Free boundary conditions. The setup of the experimental test in [Okafor et al, 1996] is shown in Figure 4.5. (No delamination is considered in this case study. The same beam with delamination will be studied in the next section.)

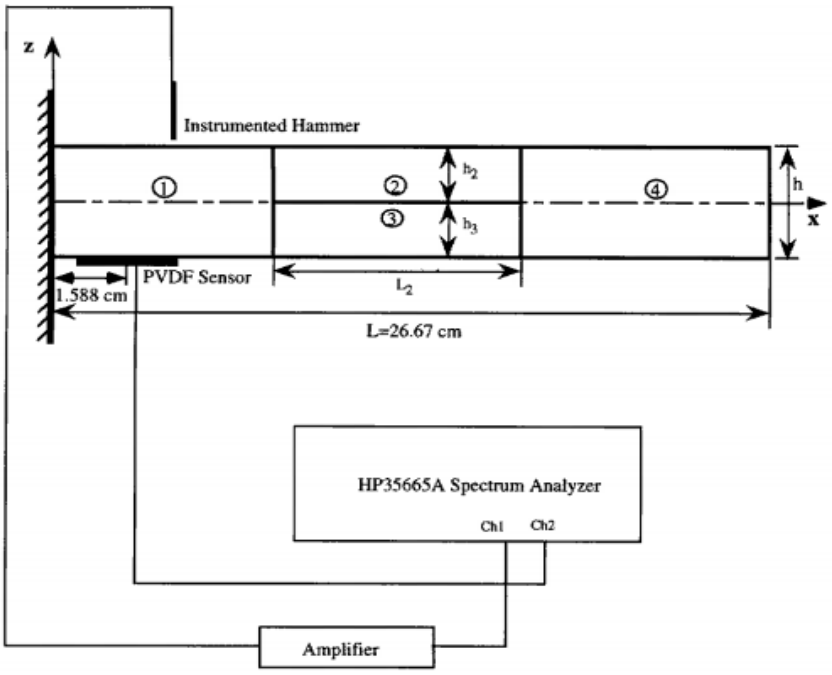

Figure 4.5: Modal testing setup from the experimental study in [Okafor et al, 1996]

Table 4.3: Natural frequencies of the composite beam considered in Example 1 in Hz

Mode Number	Current Study	(Okafor et al, 1996) Numerical study	(Okafor et al, 1996) Experimental study
1	16.16	16.17	15.00
2	101.30	101.33	97.00
3	283.63	283.76	273.00
4	555.81	556.67	535.00

The laminated composite beam shown in Figure 4.5 is modelled using 1 spectral finite element and its first four natural frequencies are calculated and compared with the numerical and experimental results from [Okafor et al, 1996] in Table 4.3.

Example 2:

A glass-polyester laminated beam of rectangular cross-section having $[45^{\circ}/45^{\circ}/45^{\circ}/45^{\circ}]$ stacking sequence is considered. This problem is also considered in [Jun et al, 2008]. The properties of the composite beam are given as follows:

$$E_1 = 37.41 \times 10^9 Pa,\ E_2 = 13.67 \times 10^9 Pa,\quad G_{12} = 5.478 \times 10^9 Pa,$$
$$G_{13} = 6.03 \times 10^9 Pa,\quad G_{23} = 6.666 \times 10^9 Pa,\quad \nu_{12} = 0.3,$$
$$\rho = 1968.9 \frac{kg}{m^3},\quad L = 0.11179m,\quad b = 12.7 \times 10^{-3}, h = 3.38 \times 10^{-3} m$$

Table 4.4: Natural frequencies of the composite beam considered in Example 2 in Hz

Mode Number	Current Study	(Jun et al, 2008)
1	398.2	397.5
2	1592.8	1581.6
3	3583.9	3526.9
4	6371.3	6193.9

The first four natural frequencies of the beam for simply-supported boundary condition are calculated and are compared with the results obtained in [Jun et al, 2008] in Table 4.4.

4.5. Natural frequencies of delaminated composite beam using Spectral Finite Element and Wittrick-Williams method

A delaminated zone is added to the laminated composite beam discussed in section 4.5, example 1. Three different delaminated cases are considered, and the results are compared with experimental and numerical results given in [Okafor et al, 1996]. The delamination is at the mid-plane of the composite beam. The distance between the center of delamination and the clamped end is 11.75 cm. Beam specimens with delamination sizes of 5.08 cm, 10.16 cm, and 15.24 cm are considered.

A total of 4 spectral elements are used to model the delaminated beam. One starting from the clamped end until the start of the delaminated zone containing 8 layers, 2 covering the top and bottom of the delaminated zone each with 4 layers and 1 covering the end of the delaminated zone until the free end of the beam containing 4 layers. The described mesh is shown in Figure 4.6:

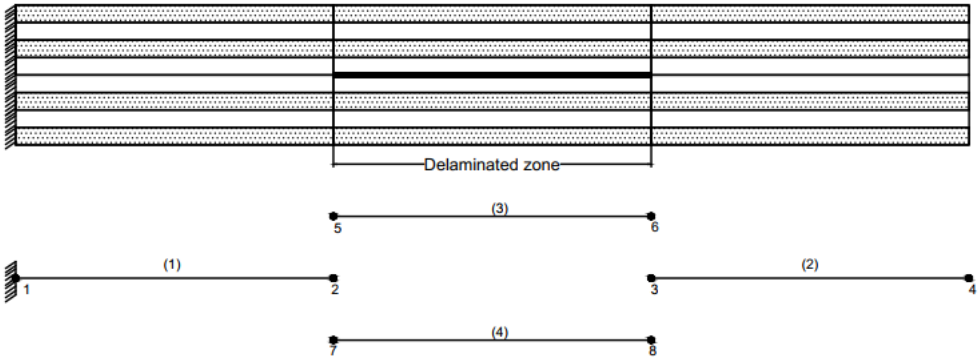

Figure 4.6: Spectral Finite Element model of the delaminated composite beam

Table 4.5: Natural frequencies of the delaminated beam in Hz (delamination size is 5.08 cm)

Mode Number	Current Study	(Okafor et al, 1996) Numerical study	(Okafor et al, 1996) experimental study
1	16.11	16.11	16
2	100.79	100.83	103
3	269.74	269.00	258
4	531.01	531.10	523

Table 4.6: Natural frequencies of the delaminated beam in Hz (delamination size is 10.16 cm)

Mode Number	Current Study	(Okafor et al, 1996) Numerical study	(Okafor et al, 1996) Experimental study
1	15.72	15.72	16
2	96.86	96.86	98
3	224.71	224.93	223
4	458.82	456.84	441

Table 4.7: Natural frequencies of the delaminated beam in Hz (delamination size is 15.24 cm)

Mode Number	Current Study	(Okafor et al, 1996) Numerical study	(Okafor et al, 1996) Experimental study
1	14.82	14.83	14
2	87.41	87.43	82
3	178.70	197.16	183
4	397.20	397.41	369

The first four natural frequencies of delaminated beams with 5.08 cm, 10.16 cm and 15.24 cm long delaminations are calculated and compared with that of the experimental and numerical studies given in [Okafor et al, 1996]. The results show a close agreement between the frequencies obtained in this study and what was obtained in previous studies.

4.6. Effect of mid-plane delamination location on the natural frequencies of laminated composite beam

Consider the delaminated beam discussed in the previous section. To investigate the effect of delamination location on the frequency of each mode, a damage model of the beam as shown in Figure 4.6 is built using spectral elements. A delaminated zone with the length of 4 cm is moved along the length of the beam from the clamped end until the free end and the first 8 frequencies of each model are captured. Figure 4.7 shows how changing the location of the delaminated area affects the first 8 modes of vibration.

The relative difference between the frequency of each mode for each damage case, is calculated using Eq. 4.3. This difference shows the percentage of frequency drop in each mode for each damage case:

$$diff_i = (1 - \frac{f_i^{fully-bonded} - f_i^{damaged}}{f_i^{fully-bonded}}) \times 100 \tag{4.3}$$

The maximum value of $diff_i$ for all the damage cases, can be interpreted as an indication of how much the i^{th} mode is affected by the delamination. Figure 4.8 shows the relative difference in frequency due to delamination location for the first 8 modes of vibration. The maximum values of the relative difference in frequencies of each mode due to delamination effect are compared with each other in Figure 4.9. Figure 4.9 shows that delamination affects higher modes of vibration much more than the lower ones.

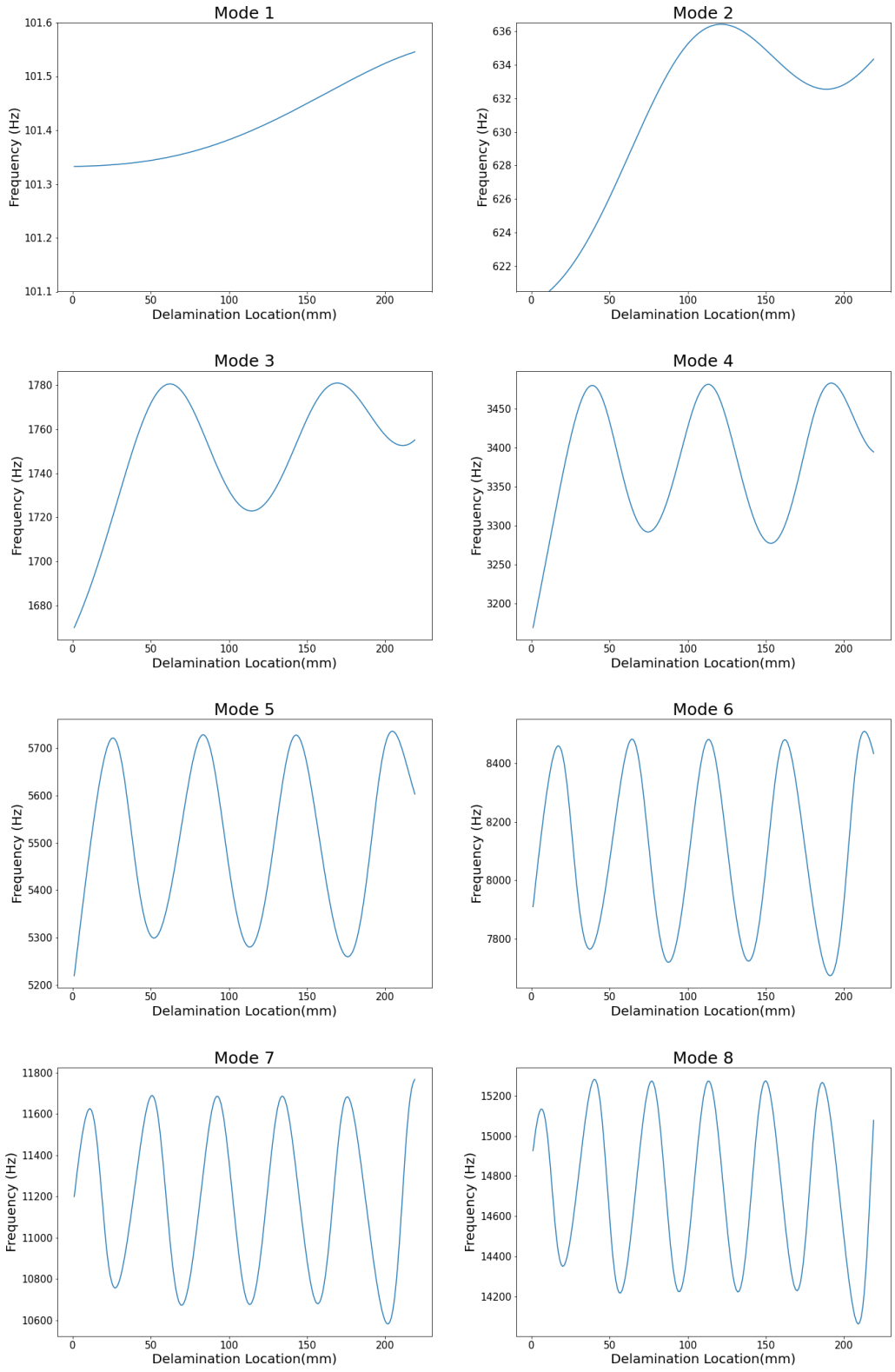

Figure 4.7: Effect of delamination location on the first 8 natural frequencies of the laminated beam

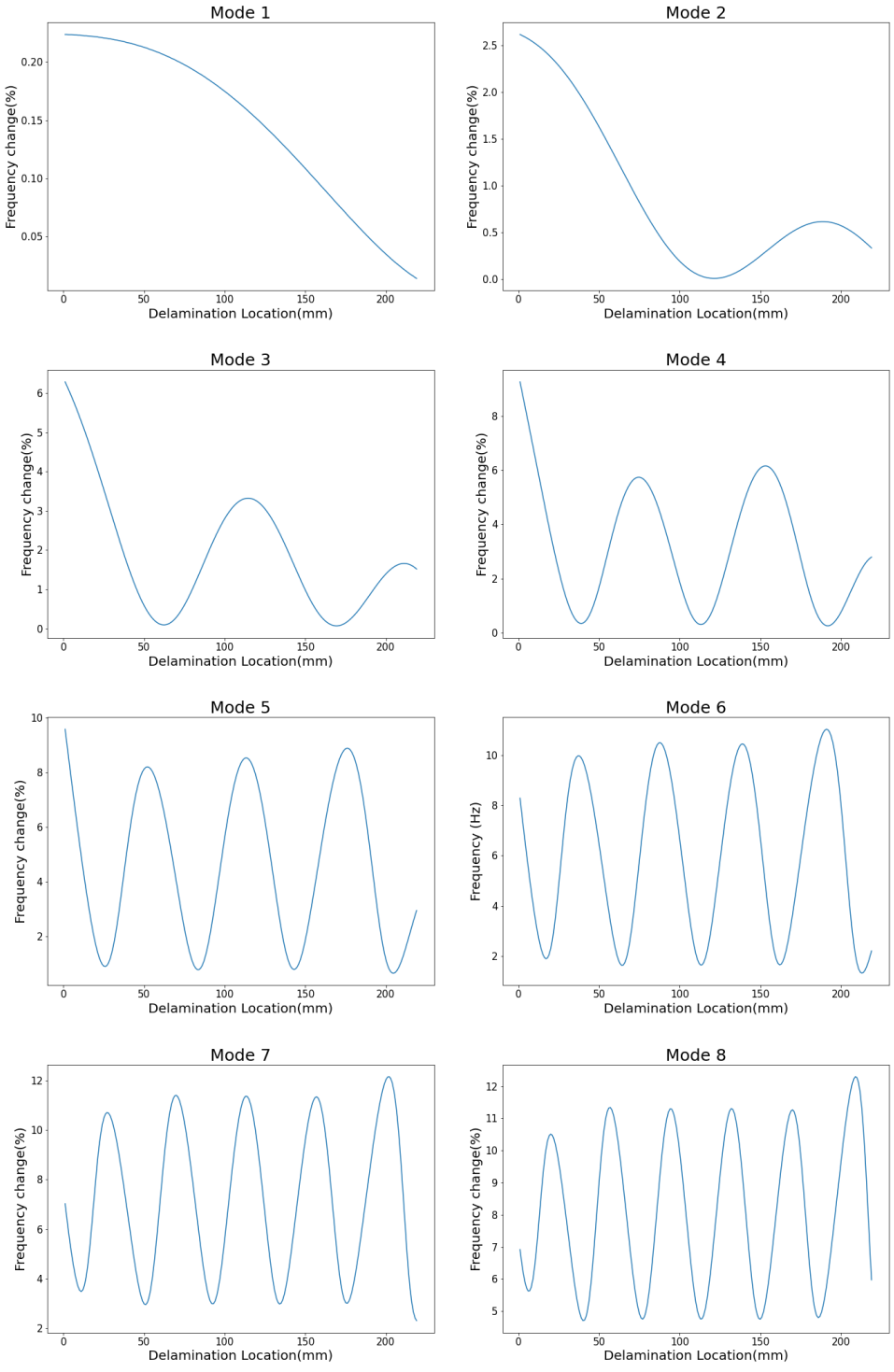

Figure 4.8: Effect of delamination location on the relative difference of the first 8 natural frequencies of the composite beam.

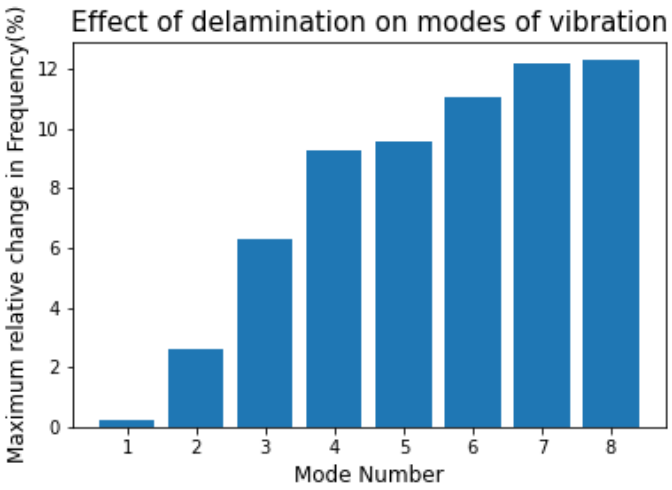

Figure 4.9: Effect of delamination on the natural frequency of the first 8 modes of vibration

4.7. Effect of friction between the top and bottom layers in the delaminated zone

As discussed in section 3.22, spring elements with axial stiffness in both X and Y directions are used to connect the top and bottom layers in the delaminated zone to bring the spectral finite element model closer to the real case. In this section, the beam discussed in section 4.6 is considered to be completely delaminated and the top and bottom layers are held together using spring elements with the stiffness matrix shown in Eq. 3.182. The number of spring elements in the delaminated zone is increased as shown in Figure 4.11 to study the effect of friction between the top and bottom layers.

Top and bottom layers can also be connected to each other using the MPC links. A pair of extra nodes are added to the top and bottom layers in the delaminated zone and the constraints in Eq. 4.4 are applied to their degrees-of-freedom.

$$\begin{Bmatrix} u_{bottom} \\ v_{bottom} \\ \theta_{bottom} \end{Bmatrix} = \begin{Bmatrix} u_{top} - \frac{h}{2}\theta_{top} \\ v_{top} \\ \theta_{top} \end{Bmatrix} \tag{4.4}$$

For example, in the second case shown in Figure 4.10 with 1 pair of extra nodes in the delaminated zone, the following constraints are applied:

$$\begin{Bmatrix} u_6 \\ v_6 \\ \theta_6 \end{Bmatrix} = \begin{Bmatrix} u_5 - \frac{h}{2}\theta_5 \\ v_5 \\ \theta_5 \end{Bmatrix} \tag{4.5}$$

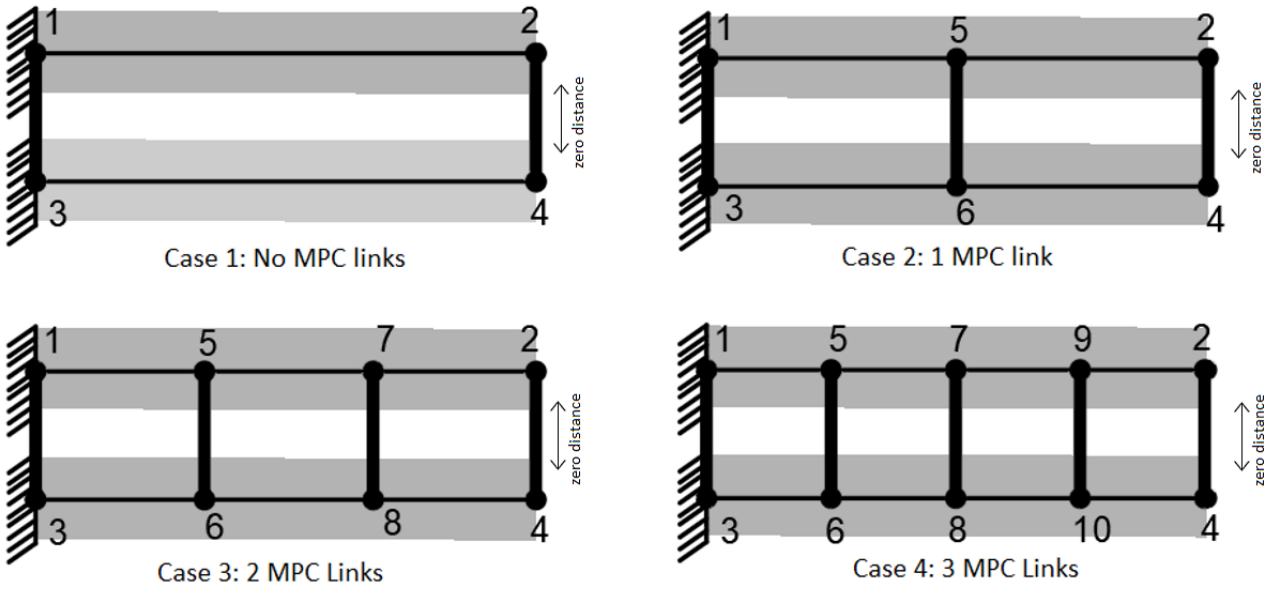

Figure 4.10: Extra MPC links to add extra stiffness in the delaminated zone

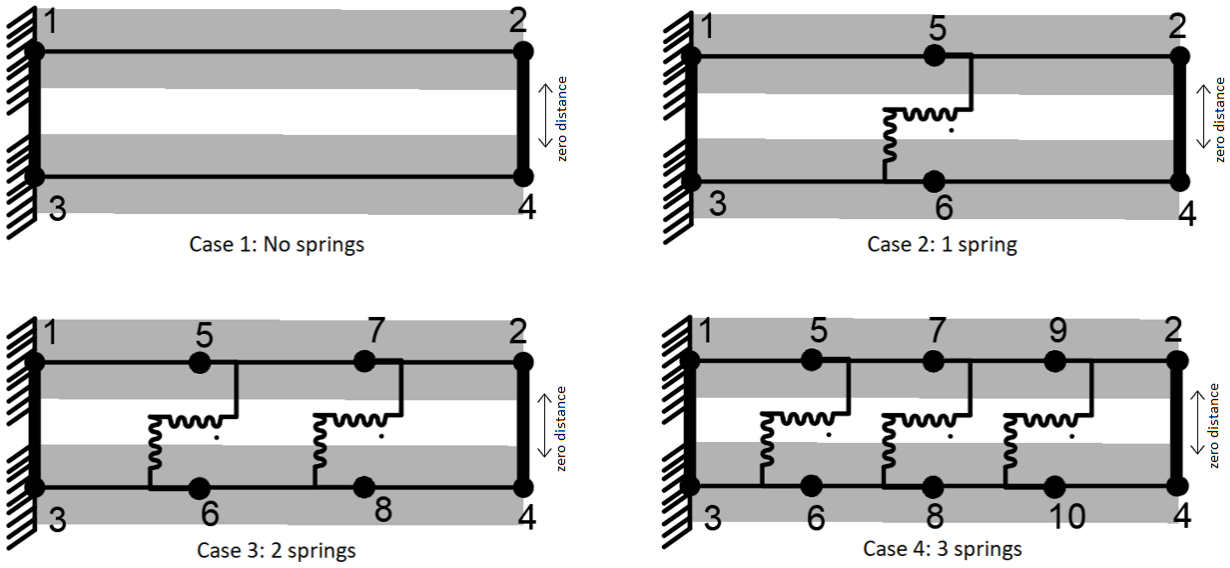

Figure 4.11: Truss elements added to add extra stiffness in the delaminated zone

Table 4.8: Comparison of natural frequencies of models with extra MPC links for the fully-delaminated and fully-bonded cases. (Hz)

Mode	Delaminated	1 MPC Link	2 MPC Links	3 MPC Links	Fully-bonded
1	11.973	14.291	15.479	15.767	16.163
2	58.368	65.150	79.773	87.222	101.296
3	64.999	162.172	181.472	212.303	283.632

Table 4.9: Comparison of natural frequencies of models with 1 extra spring element in the delaminated area for the fully-delaminated and fully-bonded cases. (Hz)

Mode Number	K_{spring} in both directions (N/m)					Fully-bonded
	0.0	1.0E+03	1.0E+06	1.0E+09	1.0E+12	
1	11.973	11.973	12.190	12.857	12.860	16.163
2	58.367	65.001	65.821	68.642	68.654	101.296
3	64.999	115.495	160.892	160.892	160.892	283.632

Table 4.10: Comparison of natural frequencies of models with 2 extra spring elements in the delaminated area for the fully-delaminated and fully-bonded cases. (Hz)

Mode Number	K_{spring} in both directions (N/m)					Fully-bonded
	0.0	1.0E+03	1.0E+06	1.0E+09	1.0E+12	
1	11.973	11.974	12.397	13.294	13.298	16.163
2	58.367	65.002	66.644	70.778	70.796	101.296
3	64.999	127.541	171.657	178.092	178.122	283.632

Table 4.11: Comparison of natural frequencies of models with 3 extra spring elements in the delaminated area for the fully-delaminated and fully-bonded cases. (Hz)

Mode Number	K_{spring} in both directions (N/m)					Fully-bonded
	0.0	1.0E+03	1.0E+06	1.0E+09	1.0E+12	
1	11.973	11.974	12.566	13.555	13.559	16.163
2	58.367	65.003	67.351	72.177	72.199	101.296
3	64.999	144.446	172.675	180.558	180.597	283.632

The first 3 natural frequencies of the cases with addition of 1, 2 and 3 Springs and 1, 2 and 3 MPC links are compared for a completely delaminated case and a fully-bonded case. It is shown in Table 4.8 that by increasing the number of MPC links, the behavior of the completely delaminated beam converges toward the fully bonded case.

In Tables 4.9, 4.10 and 4.11, the effect of adding spring elements and increasing their stiffness is studied. It is observed that by increasing the stiffness of springs and keeping the number of springs constant, frequencies get closer to the fully-bonded case and converge on a value between the completely delaminated and the fully-bonded case. It is also observed that by increasing the number of spring elements, this converged value gets closer to the frequencies of the fully-bonded case.

For both cases with MPC links and spring elements, it is observed that as the mode number is increased, frequencies converge to that of the fully-bonded case with a lower rate.

4.8. Damage detection in damaged isotropic beams using Genetic Algorithm

The damage detection algorithm explained in sections 3.16 – 3.19 is used to find damage in isotropic beams. Consider a damaged structure as shown in Figure 3.16 with the following properties of $L = 20\,in,\ L_w = 5\,in, D = 25\%$. The first three natural frequencies and mode shapes are calculated using spectral analysis. The results are taken as $\{\lambda\}^{exp}, \{\Phi\}^{exp}$ in Eq. 3.114 as simulation of a vibration test.

The Genetic Algorithm computes 8 trial solutions for each generation and generates the new generation based on the best solutions of the previous generation. The algorithm stops when the cost function of the best solution becomes zero or when the number of generations reaches a certain limit. The trial solution with the lowest cost in each generation is plotted in Figure 4.12.

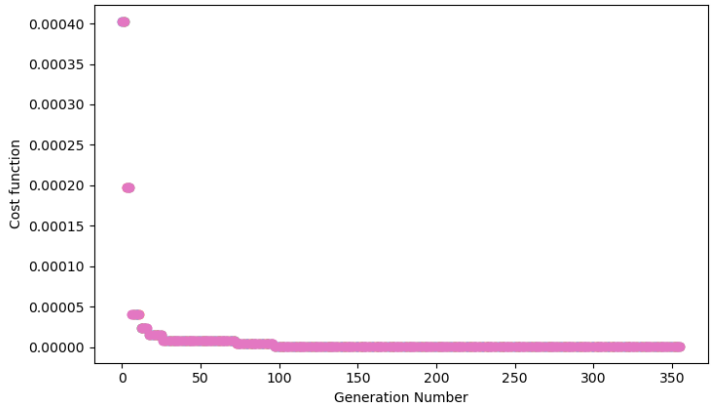

Figure 4.12: Performance of the Genetic Algorithm

The exact values for $\{L^{trial}, L_w^{trial}, D^{trial}\}$ were predicted in the 356th generation. This means that (356*8 =) 2848 possible cases were investigated until the right solution was found. Considering the constraints in Eq. 3.115 and with regards that L_w^{max} was taken as 20 as a simplifying assumption, (20*60*100 =) 120000 possible cases of damage exist. This means that the Genetic algorithm found the exact location of damage and its severity by considering only $\left(\frac{2848}{120000} * 100\right)$ 2.37% of all possible cases.

4.9. Delamination detection in delaminated composite beams using Genetic Algorithm

The algorithm explained in sections 3.16 – 3.19 is extended to work with the delaminated composite analysis program. A delamination can be addressed using two parameters, its location and its length as shown in Figure 4.13. The damage index from the previous formulation can be removed in this part and each damaged model can be referenced using only two parameters: L and Lw.

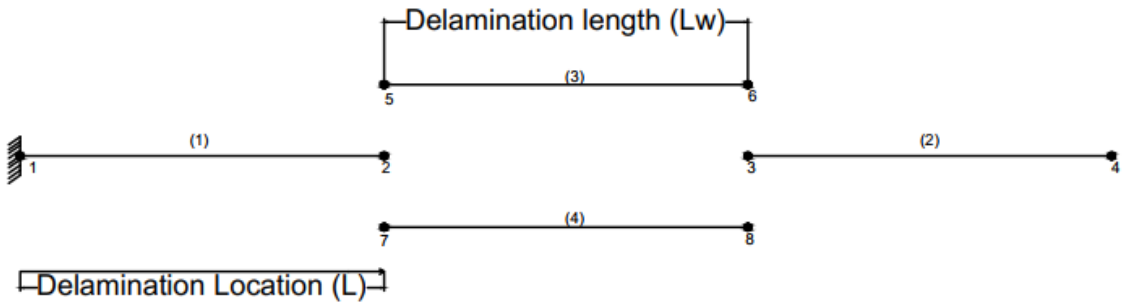

Figure 4.13: Model parameters of delaminated beam

To study the performance of the delamination detection algorithm, a delamination is introduced at 100 mm away from the clamped end of the model of the beam shown in Figure 4.6. The delamination length is assumed to be 20 mm. The first 3 modes of the delaminated model are calculated. The delamination detection algorithm is used to find the model that matches the vibration properties of the said delaminated beam with L=100mm and Lw=20mm. The performance of the damage detection program is shown in Figure 4.14. In Figure 4.14 the cost of the candidate with the lowest cost in each generation is plotted against the generation number. The updated model is found in the 22nd generation.

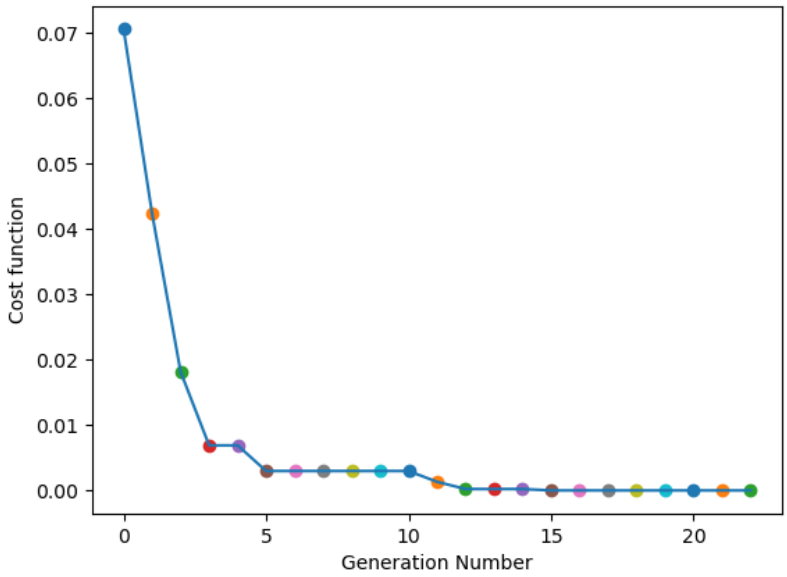

Figure 4.14: Performance of the delamination detection algorithm

To demonstrate the positive effect of having access to more modes on the performance of the damage detection program, a case study is done. Consider the same delaminated composite beam in section 4.6. 20 random damaged cases are created, and their first four natural frequencies and mode shapes are captured using spectral element model. The damage detection algorithm is used for each damage case, but only the vibration features of the first mode is fed to the algorithm and the predicted delamination length and location are stored. This process is repeated 3 more times and each time, 20 new delaminated cases are created and the first two, first three and first four vibration features are fed to the program.

The location and length of each prediction are compared with the corresponding delaminated case and if the predicted damaged model is close enough, the prediction is labeled true, otherwise it is labeled false. A prediction was assumed to be true if the difference between the delamination locations is less than 2 cm and the difference between the delamination lengths is less than 1 cm. The number of true predictions using each number of vibration modes is counted and shown in Figure 4.15.

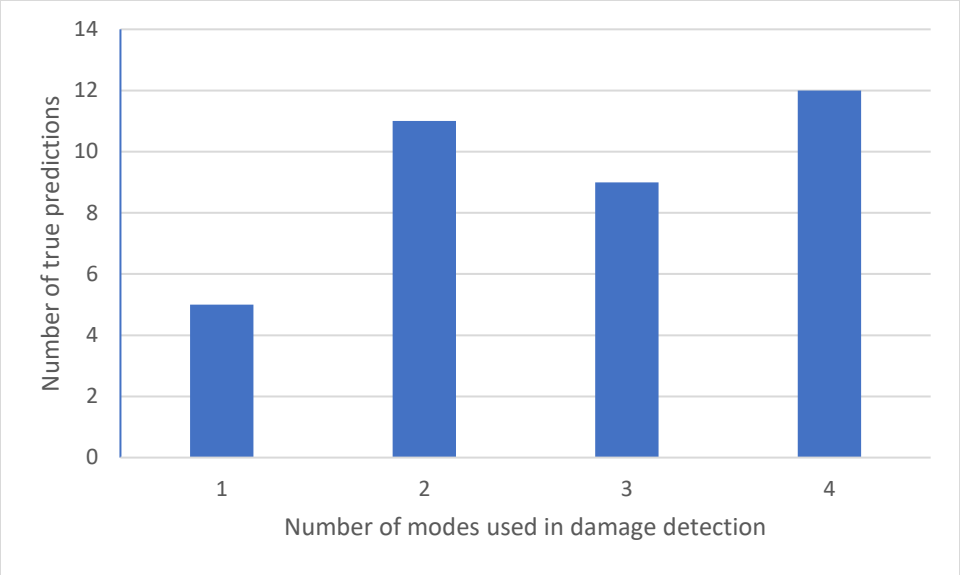

Figure 4.15: Effect of number of modes used on the performance of the damage detection algorithm

According to Figure 4.15, feeding more vibration modes to the damage detection algorithm, increases the performance of the algorithm.

Chapter 5

Conclusion and future works

A transient solution procedure was developed within the context of spectral element method and implemented for the analysis of Euler-Bernoulli beams. As Spectral Element procedure is originally developed for the steady-state dynamic solution, the developed procedure utilizes the steady-state solution to determine the transient solution. The numerical efficiency of the Spectral Element Method over the Finite Element Method, in obtaining the free vibration frequencies and mode shapes, was illustrated in case studies. The efficiency of the Spectral Element Method becomes more significant in higher frequencies which is especially important as in many cases damage effects reveal themselves only at high frequencies. Results of the dynamic analysis were employed in a genetic algorithm-based damage detection procedure. The genetic algorithm searches for the optimum of a cost function that employs the frequencies and mode shapes of the spectral element model to identify the damaged configuration, including damage location and size.

The developed spectral Euler-Bernoulli beam element was combined with spectral bar element to create a frame element with axial, transverse and rotational degrees-of-freedom at each node. The frame element was used to model the dynamic behavior of symmetric laminated composite beams. Multiple-Points-Constraints method was used to model mid-plane delamination inside the laminated composite beams. Case studies were done by comparing the natural frequencies of fully-bonded and delaminated composite beams obtained by the introduced model with that of the previous works in the literature. Effect of delamination location on natural frequencies of delaminated composite beams was studied and it was shown that delamination affects higher modes of vibration more significantly. Spring elements were used inside the delaminated zone to model the effect of extra stiffness due to the friction and cohesion between the top and bottom layers. A vibration-based delamination detection algorithm based on Genetic Algorithm was developed. The performance of the algorithm in solving inverse problems was tested by creating the model of the delaminated beam based on observed frequencies and mode shapes. The effect of having access to higher modes of vibration on the performance of the delamination detection algorithm was shown.

The major findings and observations in this study are indicated as below:

1) Application of Spectral Finite Element method as a computationally efficient tool for dynamic analysis of isotropic beams and laminated composite beams was shown.
2) A method was adopted from previous works in the literature to calculate the free vibration response of structures using steady-state solution, vibration natural frequencies and vibration mode shapes. The method was combined with the Wittrick-Williams algorithm to calculate the free vibration response.
3) A vibration-based damage detection algorithm based on the Genetic Algorithm was developed. The algorithm minimizes a cost function that was adopted from previous works in the literature using the free vibration results obtained using the dynamic stiffness matrix. The performance of the algorithm was shown by performing damage detection on damaged isotropic beams and delaminated composite beams.

The author recommends the following research works that can be pursued based on the results of this thesis:

1) Development of a Spectral Finite Element Model for unsymmetric laminated composite beams where the axial behavior is not uncoupled from the bending behavior.
2) Development of new method for calculation of J0 in the Wittrick-Williams method in cases that an analytical solution is not available. It is possible to obtain J0 by tracing the signcount of the dynamic stiffness matrix of spectral finite element model as the mesh is refined.
3) Development of a data-driven approach to improve the performance of the damage detection algorithm when real data from experimental vibration tests are used. The author believes there is a potential to integrate the proposed spectral finite element model-based damage detection algorithm with a data-driven approach to come up with a physics-guided damage detection algorithm. The physics-guided algorithm can overcome the weak performance of model-based techniques when it is subjected to experimental data and the problem of data-driven-only methods when the vibration features data set is small.

References

Allemang, Randall J. "The modal assurance criterion–twenty years of use and abuse." Sound and Vibration, Vol. 37, no. 8 (2003), pp. 14-23.

Bagchi, Ashutosh. "Updating the mathematical model of a structure using vibration data." Journal of Vibration and Control, Vol. 11, no. 12 (2005), pp. 1469-1486.

Black, Thomas Andrew. "Spectral element analysis of bars, beams, and Levy plates." PhD diss., Virginia Tech, 2005.

Cawley, Peter and Robert D.Adams. "A vibration technique for non-destructive testing of fibre composite structures." Journal of Composite Materials, Vol. 13, no. 2 (1979), pp. 161-175.

Dong, Xinjun, and Yang Wang. "Formulation and optimization algorithm comparison for the FE model updating of large-scale models." (2018). https://github.com/ywang-structures/Structural-Model-Updating

Doyle, James F. "Wave propagation in structures: Spectral Analysis Using Fast Discrete Fourier Transforms – 2nd ed". Springer, New York, NY, 1989.

Epperson, James F. "An introduction to numerical methods and analysis". John Wiley & Sons, Hoboken, New Jersey, 2013.

Friswell, M. I., J. E. T. Penny, and D. A. L. Wilson. "Using vibration data and statistical measures to locate damage in structures." The International Journal of Analytical and Experimental Modal Analysis, Vol. 9, no. 4 (1994), pp. 239-254.

Garg, A. K., D. Roy Mahapatra, S. Suresh, S. Gopalakrishnan, and S. N. Omkar. "Estimation of composite damage model parameters using spectral finite element and neural network." Composites Science and Technology, Vol. 64, no. 16 (2004), pp. 2477-2493.

Goldberg, David E., and Holland, John Henry. "Genetic algorithms and machine learning.", Addison-Wesley Publishing Company, Inc, Massachusetts, 1988.

Hao, Hong, and Yong Xia. "Vibration-based damage detection of structures by genetic algorithm." Journal of computing in civil engineering, Vol. 16, no. 3 (2002), pp. 222-229.

Ihesiulor, Obinna K., Krishna Shankar, Zhifang Zhang, and Tapabrata Ray. "Delamination detection with error and noise polluted natural frequencies using computational intelligence concepts." Composites Part B: Engineering, Vol. 56 (2014), pp. 906-925.

Jun, Li, Li Xiaobin, and Hua Hongxing. "Free vibration analysis of third-order shear deformable composite beams using dynamic stiffness method." Archive of Applied Mechanics, Vol. 79, no. 12 (2009), pp.1083-1098.

Lee, U., and J. Shin. "A frequency-domain method of structural damage identification formulated from the dynamic stiffness equation of motion." Journal of Sound and Vibration, Vol. 257, no. 4 (2002), pp. 615-634.

Lee, Usik, Sunghwan Kim, and Jooyong Cho. "Dynamic analysis of the linear discrete dynamic systems subjected to the initial conditions by using an FFT-based spectral analysis method. " Journal of sound and vibration, Vol. 288, no. 1-2 (2005), pp. 293-306.

Lee, Usik."Spectral element method in structural dynamics", John Wiley & Sons, Singapore, 2009.

Majumdar, and PM, Suryanarayan S. "Flexural vibration of beams with delamination". Journal of Sound and Vibration, Vol. 125, no. 3 (1988), pp. 441–61.

Moller, Peter W., and Olof Friberg. "Updating large finite element models in structural dynamics." AIAA journal, Vol. 36, no. 10 (1998), pp. 1861-1868.

Mottershead, John E., and M. I. Friswell. "Model updating in structural dynamics: a survey." Journal of sound and vibration 167, no. 2 (1993), pp. 347-375.

Nag, A., D. Roy Mahapatra, and S. Gopalakrishnan. Identification of delamination in composite beams using spectral estimation and a genetic algorithm. Smart Materials and Structures, Vol. 11, no. 6 (2002), pp. 899.

Okafor, A. Chukwujekwu, K. Chandrashekhara, and Y. P. Jiang. "Delamination prediction in composite beams with built-in piezoelectric devices using modal analysis and neural network." Smart materials and structures, Vol. 5, no. 3 (1996), pp. 338.

Ostachowicz, Wieslaw M. "Damage detection of structures using spectral finite element method. " Computers & structures, Vol. 86, no. 3-5 (2008), pp. 454-462.

Pardoen, Gerard C. "Effect of delamination on the natural frequencies of composite laminates." Journal of composite materials, Vol. 23, no. 12 (1989),pp 1200-1215.

Reddy, Junuthula Narasimha. "An introduction to the finite element method." McGraw-Hill, Inc, United States of America, 1989.

Tracy, John J., and Gerard C. Pardoen. "Effect of delamination on the flexural stiffness of composite laminates." Thin-Walled Structures, Vol. 6, no. 5 (1988), pp. 371-383.

Vandiver, J. Kim. "Detection of structural failure on fixed platforms by measurement of dynamic response." Journal of Petroleum Technology, Vol. 29, no. 3 (1975), pp. 305-310

Veletsos, Anestis S., and Ashok Kumar. "Steady-state and transient responses of linear structures." Journal of Engineering Mechanics, Vol. 109, no. 5 (1983), pp. 1215-1230.

Clough, R. W. and Penzien, J. "Dynamics of Structures", Computers & Structures, Inc, Berkeley, CA, USA, 1995.

Williams, F. W., and W. H. Wittrick. "An automatic computational procedure for calculating natural frequencies of skeletal structures." International Journal of Mechanical Sciences, Vol. 12, no. 9 (1970), pp. 781-791.